Mineral Oxides Change the Atmospheric Reactivity of Soot: NO2 Uptake under Dark and UV Irradiation Conditions

ARTICLE *in* THE JOURNAL OF PHYSICAL CHEMISTRY A · NOVEMBER 2013

Impact Factor: 2.69 · DOI: 10.1021/jp407914f · Source: PubMed

7 AUTHORS, INCLUDING:

Manolis N Romanias
Ecole des Mines de Douai
25 PUBLICATIONS **99** CITATIONS
SEE PROFILE

Yuri Bedjanian
CNRS Orleans Campus
67 PUBLICATIONS **861** CITATIONS
SEE PROFILE

Aurea Andrade-Eiroa
French National Centre for Scientific Research
27 PUBLICATIONS **231** CITATIONS
SEE PROFILE

Roya Shahla
CNRS Orleans Campus
5 PUBLICATIONS **8** CITATIONS
SEE PROFILE

THE JOURNAL OF PHYSICAL CHEMISTRY A

Article

pubs.acs.org/JPCA

Mineral Oxides Change the Atmospheric Reactivity of Soot: NO_2 Uptake under Dark and UV Irradiation Conditions

Manolis N. Romanias,*[,†] Yuri Bedjanian,[†] Aristotelis M. Zaras,[†] Aurea Andrade-Eiroa,[†] Roya Shahla,[†] Philippe Dagaut,[†] and Aggelos Philippidis[‡]

[†]Institut de Combustion, Aérothermique, Réactivité et Environnement (ICARE), CNRS-INSIS, Université d'Orléans, Orléans Cedex 2, France

[‡]Institute of Electronic Structure and Laser, Foundation for Research and Technology-Hellas (IESL-FORTH), P.O. Box 1385, GR 711 10 Heraklion Crete, Greece

Supporting Information

ABSTRACT: The heterogeneous reactions between trace gases and aerosol surfaces have been widely studied over the past decades, revealing the crucial role of these reactions in atmospheric chemistry. However, existing knowledge on the reactivity of mixed aerosols is limited, even though they have been observed in field measurements. In the current study, the heterogeneous interaction of NO_2 with solid surfaces of Al_2O_3 covered with kerosene soot was investigated under dark conditions and in the presence of UV light. Experiments were performed at 293 K using a low-pressure flow-tube reactor coupled with a quadrupole mass spectrometer. The steady-state uptake coefficient, γ_{ss}, and the distribution of the gas-phase products were determined as functions of the Al_2O_3 mass; soot mass; NO_2 concentration, varied in the range of $(0.2-10) \times 10^{12}$ molecules cm^{-3}; photon flux; and relative humidity, ranging from 0.0032% to 32%. On Al_2O_3/soot surfaces, the reaction rate was substantially increased, and the formation of HONO was favored compared with that on individual pure soot and pure Al_2O_3 surfaces. Uptake of NO_2 was enhanced in the presence of H_2O under both dark and UV irradiation conditions, and the following empirical expressions were obtained: $\gamma_{ss,BET,dark} = (7.3 \pm 0.9) \times 10^{-7} + (3.2 \pm 0.5) \times 10^{-8} \times RH$ and $\gamma_{ss,BET,UV} = (1.4 \pm 0.2) \times 10^{-6} + (4.0 \pm 0.9) \times 10^{-8} \times RH$. Specific experiments, with solid sample preheating and doping with polycyclic aromatic hydrocarbons (PAHs), showed that UV-absorbing organic compounds significantly affect the chemical reactivity of the mixed mineral/soot surfaces. A mechanistic scheme is proposed, in which Al_2O_3 can either collect electrons, initiating a sequence of redox reactions, or prevent the charge-recombination process, extending the lifetime of the excited state and enhancing the reactivity of the organics. Finally, the atmospheric implications of the observed results are briefly discussed.

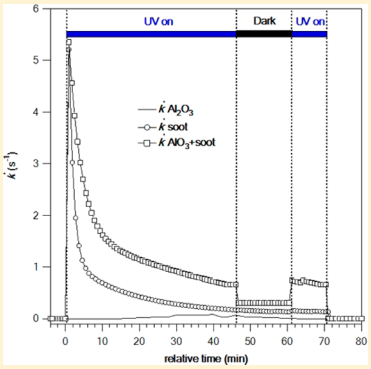

1. INTRODUCTION

Soot particles are formed from the incomplete combustion of fuels (e.g., burning of biomass, operating of engines and furnaces). They are composed of elementary carbon and numerous organic compounds.[1] The atmospheric lifetime of soot is estimated to be ~1 week.[2] Black-carbon global emissions exceed 20.0 Tg/year, with the main fraction coming from the combustion of fossil fuels.[3] The major direct impact of soot on the environment and climate is the scattering/absorption of sunlight. Indirectly, soot participates in the formation of clouds, acting as condensation nuclei. Both processes can significantly influence the radiation balance of the planet. In addition, because its porous nature provided large surface areas, soot can participate in heterogeneous reactions with gas-phase compounds, influencing the chemical composition of the troposphere.[4]

According to recent estimations, every year, 1600 Tg of mineral dust is released into the atmosphere,[3a,5] representing the largest mass emission rate of aerosol particles at a global scale.[3a] Although the primary sources are arid regions, because of global air circulation, mineral particles undergo long-range transportation to remote areas. The major source of mineral dust is the African continent mainly because of the presence of the Sahara desert, contributing ~62% of the total emissions.[6] Dust surfaces can provide the seedbed for trace gas molecules adsorption/reaction and, therefore, are considered to play a key role in the transformation and environmental fate of many atmospheric species.[7]

Recent field studies have reported the existence of mixed aerosols.[8] Kim et al.[8c] observed internal mixing of mineral dust with industrial soot particles. In particular, after long-range transportation over polluted areas, mineral dust originating from North China was enriched with substantial concentrations of elemental and organic carbon.[8c] Also, Hand et al.[8a] verified the internal mixing of dust with soot during a field campaign performed in 2006 over North Africa between December and February, when the maximum seasonal emissions of anthropogenic biomass-burning aerosols occur.[8a] The authors

Received: August 7, 2013
Revised: November 4, 2013
Published: November 4, 2013

observed that up to a third of soot particles were internally mixed with dust. The blending of aerosol surfaces could influence not only their optical properties, as has been already observed, but also the chemical reactivity.

Although the reaction of trace gases with pure soot and pure mineral surfaces has been extensively studied in the past,[1b,c,9] information about the reactivity of atmospheric trace gases with mixed aerosol surfaces is basically lacking. The aim of the current study was to investigate the chemical reactivity of mineral aerosols covered with soot. γ-Al_2O_3 was used as a model compound to mimic mineral aerosols because it is the second most abundant component (after SiO_2) of mineral dust. The heterogeneous interactions of NO_2 with solid surfaces of pure γ-Al_2O_3, pure kerosene soot, and γ-Al_2O_3 covered with kerosene soot were investigated under dark conditions and in the presence of UV light. Experiments were performed at 293 K using a low-pressure flow-tube reactor coupled with a quadrupole mass spectrometer. The steady-state uptake coefficient, γ_{ss}, and the yields of the gas-phase products were determined as functions of Al_2O_3 mass; soot mass; NO_2 concentration, varied in the range of $(0.2-10) \times 10^{12}$ molecules cm^{-3}; irradiance intensity; relative humidity, ranging from 0.0032% to 32%; surface heating; and doping with PAHs. Finally, an electron-transfer-initiated mechanism of NO_2 reaction with mixed soot/Al_2O_3 surfaces is proposed. To our knowledge, this is the first laboratory study dealing with the reactivity of mixed mineral/soot aerosol.

2. EXPERIMENTAL SECTION

2.1. Preparation of Al_2O_3 Surfaces. Solid Al_2O_3 films were deposited on the outer surface of a Pyrex tube (0.9-cm outer diameter) from a γ-Al_2O_3 (Alfa Aesar, ~20-nm particle diameter) suspension in ethanol. Prior to film deposition, the Pyrex tube was treated with hydrofluoric acid and washed with distilled water and ethanol. Then, the tube was immersed into the suspension, withdrawn, and dried with a fan heater. To eliminate possible residual traces of ethanol, prior to uptake experiments, the freshly prepared Al_2O_3 samples were heated at 150−170 °C under pumping for 20−30 min. Regarding experiments in which Al_2O_3 surfaces were covered with soot, no preheating of the coated surface was performed, unless noted otherwise.

2.2. Preparation of Soot/Al_2O_3-Soot Surfaces. A flat-flame burner was used for the combustion of kerosene fuel under well-characterized and controlled conditions.[9q] A simplified scheme of the soot production and collection system was presented elsewhere.[9q] Kerosene was pumped by a Gilson pump with a flow rate of 140 μL/min and subsequently driven inside a vaporizer, where it was initially mixed with a N_2 jet stream, atomized, and then vaporized into the heating chamber of the vaporizer. Afterward, the N_2/fuel mixture was further diluted with a constant flow of N_2 and O_2 inside the tubular volume of the burner. The flows of N_2 and O_2 were controlled by flow meters (MKS Instruments); thus, a known fuel/oxygen mixture was supplied to the burner. The head of the burner was isolated using a cross-type cylindrical Pyrex tube, to prevent flame perturbations from external air movements. An additional flow of nitrogen into the tube surrounding the burner was used to prevent external oxygen diffusion.

Soot samples were deposited on the outer surface of clean or Al_2O_3-precovered Pyrex rods tubes, for the preparation of surfaces of pure soot or Al_2O_3 covered with soot, respectively. The rods were introduced 4 cm above the head of the burner perpendicular to the flame axis, rotated, and moved through the flame. The sampling Pyrex tube was thermostatted at 45 °C by circulating water inside the tube. This allowed soot samples with reproducible PAH contents to be obtained.[10] To determine the soot mass in mixed soot/mineral samples, separate experiments were performed in which we measured soot deposition rate on a Pyrex tube under stabilized combustion conditions. In these experiments, soot was initially collected, then mechanically removed from the support tube, and finally weighed with a high-accuracy mass balance. For fixed flame richness (Φ, defined as the fuel/oxygen ratio multiplied by the stoichiometric coefficient of oxygen), the mass of collected soot was found to depend linearly on the sampling time. This is shown in Figure 1, where the total mass

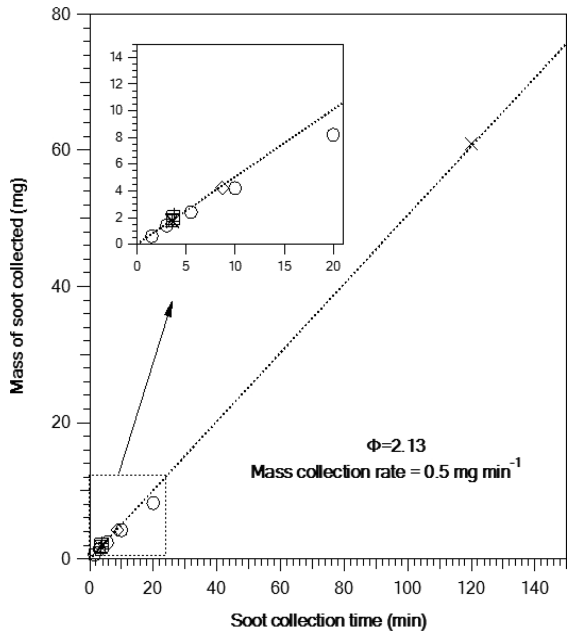

Figure 1. Total mass of deposited soot versus collection time. Different symbols correspond to experiments performed on different days. The dotted line is a linear through-origin fit of the experimental data.

of deposited soot is plotted as a a function of the collection time. Different symbols correspond to soot collection experiments performed on different days. These data indicate the good repeatability of the soot production and collection protocol and provide a soot mass collection rate of 0.50 ± 0.05 mg/min for a flame richness of Φ = 2.13 (calculated with $C_{11}H_{22}$ as the molecular formula of kerosene). This allowed the calculation of the soot mass content in the mixed Al_2O_3/soot samples (see Results and Discussion). The Brunauer−Emmett−Teller (BET) surface areas of Al_2O_3 and soot were measured with a Quantacrome Nova 2200e gas sorption analyzer using N_2 (>99.999%) as the adsorbate gas. Values of 200 ± 30 and 110 ± 20 m^2 g^{-1} were obtained for Al_2O_3 and kerosene soot, respectively.

2.3. Experimental Setup. The heterogeneous interaction of NO_2 with the solid surfaces was studied using a flow-tube reactor (FT), operated under laminar-flow conditions and coupled with a modulated molecular-beam quadrupole mass spectrometer (QMS) for the detection of gas-phase species. The FT/QMS technique has been extensively used to study the heterogeneous interactions between gas and bulk aerosol

surfaces;[11] thus, only a brief description of the experimental setup is presented here. The experimental setup consisted of three intrinsically linked parts: a gas storage/supply vacuum line, a flow-tube reactor, and a differentially pumped stainless steel high-vacuum chamber containing the quadrupole mass spectrometer (Balzers, QMG 420). The vacuum line was made exclusively of glass and consisted of calibrated volume storage flasks where the gas-phase reactants were stored. The supply of the gas-phase species inside the reactor was controlled by low-flow metering valves (Swagelok). Furthermore, four flow meters with a maximum flow rate 500 cm^3/min were contained in the gas line and connected to the reactor to regulate the flow of He, which was used as the carrier gas.

The flow-tube reactor (Figure S1, Supporting Information) was used in a coaxial configuration. It consisted of a Pyrex tube (40-cm length and 2.4-cm internal diameter) with a jacket for circulation of the thermostatted liquid. The Pyrex tube with the deposited surfaces was introduced into the main reactor along its axis. This tube could be moved through the outer tube of the injector, allowing for the variation of the length of the solid sample exposed to NO_2 and, consequently, the reaction time (t, defined as the ratio of the sample length to the flow rate). Externally, the reactor was surrounded by six UV lamps (Sylvania BL350, 8 W) with a broad UV emission spectrum (315−400 nm). The UV lamps were installed in an aluminum light-tight box covering the main reactor. The irradiance intensity in the reactor was characterized by direct measurements of the NO_2 photolysis frequency, J_{NO_2}, as a function of the number of lamps switched on.[12] It should be noted that, under the experimental conditions of the present study, the photolysis of NO_2 (as well as of HONO, observed as a reaction product) in the gas phase was negligible. The gas-phase molecules sampled from the flow reactor were modulated by a rotating disk chopper (35 Hz), ionized through impact with high-energy electrons (30 eV) emitted by the ion source of the mass spectrometer and detected using a secondary electron multiplier. Subsequently, mass spectrometric signals were filtered and amplified with a lock-in amplifier and recorded for further analysis.

2.3.1. Determination of Gas-Phase Concentrations. The concentrations of NO_2 and NO were calculated from their flow rates measured by recording the pressure drop in the calibrated-volume storage flasks and detecting the NO_2 and NO mass spectrometric intensities at their parent peaks of m/z = 46 and 30, respectively. The absolute concentrations of HONO were determined by its chemical conversion to NO_2 through the fast reaction with F atoms, with subsequent detection and measurement of the NO_2 concentration formed[13]

$$F + HONO \rightarrow HF + NO_2 \quad (1)$$

Note that HONO was generated through the heterogeneous reaction of HCl with $NaNO_2$

$$HCl + NaNO_2 \rightarrow HONO + NaCl \quad (2)$$

HCl (5% in He) was flowed through a column containing $NaNO_2$ crystals, and the heterogeneously formed HONO was injected through the reactor side arm and detected at its parent peak as $HONO^+$ (m/z = 47). Finally, H_2O vapors were introduced into the flow reactor by passing 40 cm^3/min of He through a thermostatted glass bubbler containing deionized water. The partial pressure of water in the reactor was determined by calculating the H_2O flow rate from the total (H_2O + He) and H_2O vapor pressures in the bubbler and the measured flow rate of He through the bubbler. The partial pressure of water vapor in the bubbler was measured with a Vaisala DRYCAP DMT340 dew-point transmitter.

2.3.2. Measurement of the Uptake Coefficient. The uptake coefficient of NO_2 on the deposited surfaces is given by the expression

$$\gamma = \frac{4k'}{\omega}\frac{V}{S} \quad (I)$$

where k' is the first-order rate coefficient of NO_2 loss (s^{-1}) in the "kinetic regime" (see below), ω is the average molecular speed (cm s^{-1}), V is the volume of the reaction zone (cm^3), and S is the surface area of the deposited sample participating in the reaction (cm^2). Under specified experimental conditions, both ω and V were known parameters of the system; therefore, only k' and S had to be determined experimentally.

The rate coefficient of NO_2 loss on a solid surface in the kinetic regime, k', can be directly measured from a typical experiment only when the uptake of the gas molecules is not limited by their diffusion from the reactor volume toward the reactive surface. Under these conditions, which define the kinetic regime, no further analysis is required for the determination of k', and it can be directly measured using the equation ($k' = k_{obs}$)

$$k_{obs} = -\frac{d\ln([NO_2])}{dt} = \frac{\ln\left(\frac{I_0}{I_r}\right)\nu}{L} \quad (II)$$

where I_0 and I_r are the MS signal intensities corresponding to the initial concentration of NO_2 before and after contact with the solid sample, respectively; ν is the flow velocity in the reaction zone (40−100 cm s^{-1}); and L (cm) is the length of the solid surface exposed to NO_2. When an effective heterogeneous loss leads to a significant local depletion of the gas-phase molecules close to the surface, their diffusion from the volume of the reactor toward the surface becomes rate-limiting, and corresponding corrections should be applied to measured values of k'.[11a] In the present study, the uptake was measured under steady-state uptake conditions (after 45−75 min of sample exposure to NO_2). The measured values of k' were less than 3 s^{-1}, leading to negligible diffusion corrections (<2%) under the experimental conditions used.

2.4. Analysis of Solid Samples. The determination of PAH compounds on soot was performed using a reverse-phase high-performance liquid chromatography (HPLC) system (Shimadzu Corporation) equipped with ultraviolet and fluorescence detectors. Acetonitrile (Carlo Erba reagents, LC/MS quality) was used as the solvent for the extraction of the soot organic fraction. Subsequently, the solution was filtered twice with a polytetrafluoroethylene (PTFE) filter (Alltech, 0.2-μm pore size) and finally analyzed.

The optoelectronic properties of solid samples were examined in the wavelength range of 220−2000 nm using a Perkin-Elmer Lambda 950 UV−vis−NIR spectrometer.

3. RESULTS AND DISCUSSION

The main focus of the current work was the kinetic study and product analysis of the heterogeneous interaction of NO_2 with Al_2O_3 surfaces covered with kerosene soot. However, prior to this investigation, for comparison purposes, it was necessary to test separately the reactions of NO_2 with pure Al_2O_3 and with pure soot under the same experimental conditions.

3.1. Interaction of NO_2 with Pure Al_2O_3. The time dependence of the NO_2 loss rate on 11.6 mg of Al_2O_3 under dark and UV irradiation conditions is presented in Figure 2

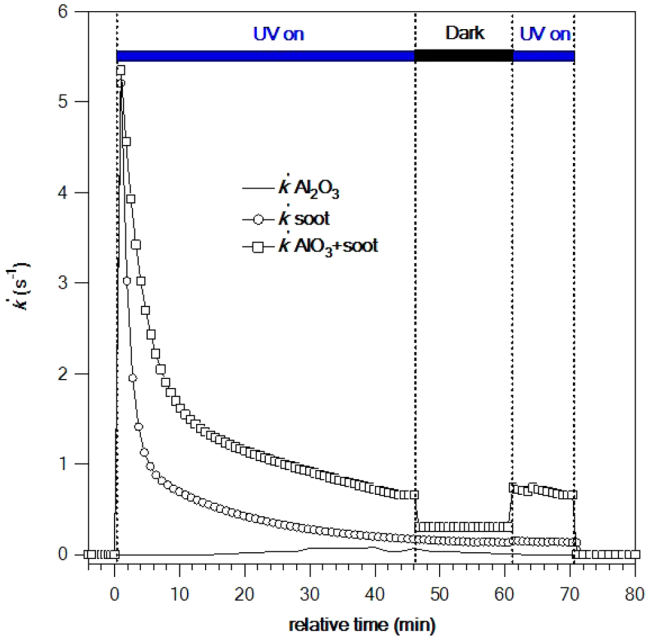

Figure 2. Dependence of NO_2 loss rate, k', on exposure time of reactive surface: solid line, 11.6 mg of pure Al_2O_3; circles, 2 mg of pure soot; squares, 11.6 mg of Al_2O_3 covered with 2 mg of soot. Experiments were performed at T = 293 K, RH ≈ 5%, and $[NO_2] \approx 2 \times 10^{12}$ molecules cm^{-3}. Solid samples were introduced into the reaction zone at t = 0 in the presence of UV light (J_{NO_2} = 0.012 s^{-1}). Lights were turned off and on at 45 and 60 min, respectively. Samples were withdrawn from the reaction zone after 70 min.

(solid line). At t = 0 and under UV light irradiation conditions, the Al_2O_3 surface was introduced into the reaction zone and exposed to NO_2; however, no measurable loss of NO_2 was observed. Switching off the lights at t = 45 min also had no impact on the uptake. Finally, at t = 70 min, the Al_2O_3 surface was removed from the reaction zone. Similar uptake experiments were performed with lower Al_2O_3 masses (down to 0.026 mg cm^{-1}). In all cases, the values of k' were extremely low and close to the detection limit of our technique; therefore, only an upper limit for k' can be given. Under dark and UV irradiation conditions (zero and six UV lamps on, respectively), a safe upper limit of $\gamma_{ss}(Al_2O_3) < 4 \times 10^{-8}$ can be given, using the BET surface area of Al_2O_3. The obtained value is in agreement with previous studies, where the uptake was found to be lower than 2×10^{-8}.[9aa]

3.2. Interaction of NO_2 with Pure Soot. The time dependence profile of the rate coefficient of NO_2 loss on 2 mg of pure soot is also presented in Figure 2 (open circles). A gradual decrease of k' with time due to surface deactivation can be observed. The irradiation of the surface did not accelerate the reaction, because no change was detected at t = 45 min and t = 60 min when the lights were switched off and on, respectively. In addition, a series of experiments was conducted in which the uptake was measured as a function of the thickness of soot samples exposed to NO_2. The objective was to determine the surface area of the solid film involved in the interaction. Experiments were performed at a temperature (T) of 293 K, a relative humidity (RH) of 5% , and a NO_2 concentration ($[NO_2]$) of $\sim 2 \times 10^{12}$ molecules cm^{-3}. The results are presented in Figure S2 (Supporting Information), where the geometric uptake coefficient is plotted as a function of the soot mass deposited per unit length of the support tube. The linear dependence of the uptake coefficient on the soot mass suggests that the entire surface area of the solid sample is accessible to NO_2 and, consequently, that the BET surface area should be applied for the determination of the true uptake coefficient. The slope of the linear fit through the origin to the experimental data provides a value for the steady-state uptake coefficient of NO_2 under the current experimental conditions (T, RH, $[NO_2]$) of γ_{ss}(soot) = $(4.9 \pm 0.8) \times 10^{-7}$, where the given uncertainty includes the precision of the fit and the uncertainties in the BET surface area and in the measurements of k'. Concerning reaction products, HONO and NO were detected in the gas phase with yields of ∼20% and ∼70%, respectively. The yield of the gas-phase products was determined as the ratio of the concentration product formed to the concentration of NO_2 consumed: product yield = $\Delta[\text{product}]/\Delta[NO_2]$. In the solid phase, nitro-PAHs were identified but not quantified. A detailed list of PAHs present in pure kerosene soot and formed upon treatment with NO_2 is provided in Table S1 (Supporting Information). Nitrochrysene and nitrocorannulene were the only nitro compounds detected on fresh soot. After treatment with NO_2 under dark conditions, 1-nitropyrene, 9-nitroanthracene, 1-nitrofluoranthrene, and 3-nitrofluoranthrene were formed, and the complete consumption of 1-hydroxypyrene was observed.

3.3. Interaction of NO_2 with Al_2O_3 Covered with Soot. In this series of experiments, the reaction of NO_2 with soot-covered Al_2O_3 surfaces was tested. The loss rate of NO_2 is presented as a function of exposure time in Figure 2, where 11.6 mg of Al_2O_3 covered with 2 mg of soot [the mass of soot

Table 1. Summary of Experimental Data[a]

sample	NO yield dark	NO yield UV[b]	HONO yield dark	HONO yield UV[b]	NO_2 taken up[c] (10^{13} molecules cm^{-2})	$\gamma_{ss,BET}$ (10^{-7}) dark	$\gamma_{ss,BET}$ (10^{-7}) UV[b]
pure soot	0.70 ± 0.14		0.20 ± 0.06		4.57 ± 1.37	4.39 ± 0.76	
pure soot preheated at 350 °C	0.32 ± 0.06		0.53 ± 0.11		8.99 ± 2.95	9.46 ± 1.91	
soot + PAHs	0.38 ± 0.08	0.53 ± 0.11	0.43 ± 0.10		3.94 ± 1.18	3.96 ± 0.79	7.12 ± 1.42
Al_2O_3 + soot	0.3 ± 0.06		0.6 ± 0.12		14.15 ± 4.20	7.93 ± 1.48	14.00 ± 2.80
Al_2O_3 + soot preheated at 350 °C	0.27 ± 0.06		0.20 ± 0.06		7.42 ± 2.23	3.87 ± 0.77	
Al_2O_3 + soot + PAHs	0.17 ± 0.05	0.41 ± 0.09	0.48 ± 0.10		20.61 ± 6.20	14.77 ± 2.95	27.88 ± 5.58

[a]RH = 5%, T = 293 K, $[NO_2] \approx 2 \times 10^{12}$ molecules cm^{-3}, Al_2O_3 = 11.6 mg, and soot = 2 mg. [b]Results under UV light correspond to J_{NO_2} = 0.012 s^{-1}. [c]NO_2 taken up after 45 min of exposure under dark conditions. For pure soot and Al_2O_3 + soot, the BET surface area of soot was used.

dx.doi.org/10.1021/jp407914f | J. Phys. Chem. A 2013, 117, 12897−12911

deposited was controlled by the soot collection time (Figure 1)] was exposed to a NO_2 concentration of ~2 × 10^{12} molecules cm^{-3} (squares). Note that the mass of solid used is the sum of the masses deposited in the experiments with pure Al_2O_3 and pure soot also presented in this figure. The observed data clearly demonstrate that the uptake of NO_2 on the mixed Al_2O_3/soot surface was significantly higher than the sum of the contributions of its constituents. In particular, the values of the rate coefficient recorded under UV irradiation were a factor of 3−4 higher than the sum of the k' values observed on the individual surfaces. Even under dark conditions, the uptake was enhanced by a factor of 2 compared with that on the pure substrates (Table 1). Furthermore, the effect of UV irradiation on the NO_2 uptake can be clearly observed t = 45 min and t = 60 min, when the lights were turned off and on, respectively. Regarding the products, 60% HONO and 30% NO were detected in the gas phase (Table 1), indicating that HONO production is favored on the soot-covered Al_2O_3 surface compared with the pure soot surface.

3.3.1. Dependence on Al_2O_3 Mass. To investigate the role of the deposited Al_2O_3 substrate, a series of experiments was carried out with varying masses of Al_2O_3 and a fixed mass of soot of ~2 mg. The results are summarized in Figure 3. It was found that variation of the mass of Al_2O_3 by a factor of 5 had no impact on the rate of NO_2 loss under both dark and UV irradiation conditions (Figure 3a). In addition, the number of NO_2 molecules lost on the surface was also invariant with respect to the Al_2O_3 mass within the range of experimental uncertainties (Figure 3b). These data seem to indicate that, although the presence of Al_2O_3 is necessary to accelerate the heterogeneous reaction, its mass (or coverage thickness) does not influence the uptake process. Consequently, in the following experiments on the measurements of the NO_2 uptake coefficient on soot-covered Al_2O_3, only the mass of soot was considered, that is, only the soot surface area was used for the calculation of the uptake coefficients.

Despite the kinetics and the surface coverage, the product yields were also determined. The results are displayed in Figure 3c, where the yields of the detected products, HONO and NO, are presented as functions of the Al_2O_3 mass. Solid and open points denote experiments under dark and UV light conditions, respectively, whereas solid lines were drawn just to guide the eyes and have no physical meaning. For comparison purposes, the yields of the products for pure soot are also presented (zero Al_2O_3 mass). As one can see, although the NO_2 uptake was found to be independent of the Al_2O_3 mass, a trend of increasing HONO yield and decreasing NO yield with increasing Al_2O_3 content in the mixed sample was observed. A possible explanation for this observation could be the involvement of the formed HONO in secondary reactions with soot and Al_2O_3 surfaces.

3.3.2. Dependence on Soot Mass. In this series of experiments, the dependence of k' on the soot coating was investigated. Experiments were performed at a temperature (T) of 293 K, a relative humidity (RH) of 5% , and a NO_2 concentration ($[NO_2]$) of ~2 × 10^{12} molecules cm^{-3} covering 11.6 mg of Al_2O_3 with different amounts of soot. The objective was to determine the limit at which further covering of the Al_2O_3 with soot caused no change in the uptake rate upon irradiation. This would be an indication that Al_2O_3 was no longer accessible and did not participate in the reaction mechanism, so that the values of uptake measured above this limit should reflect the interaction of NO_2 with pure soot. The

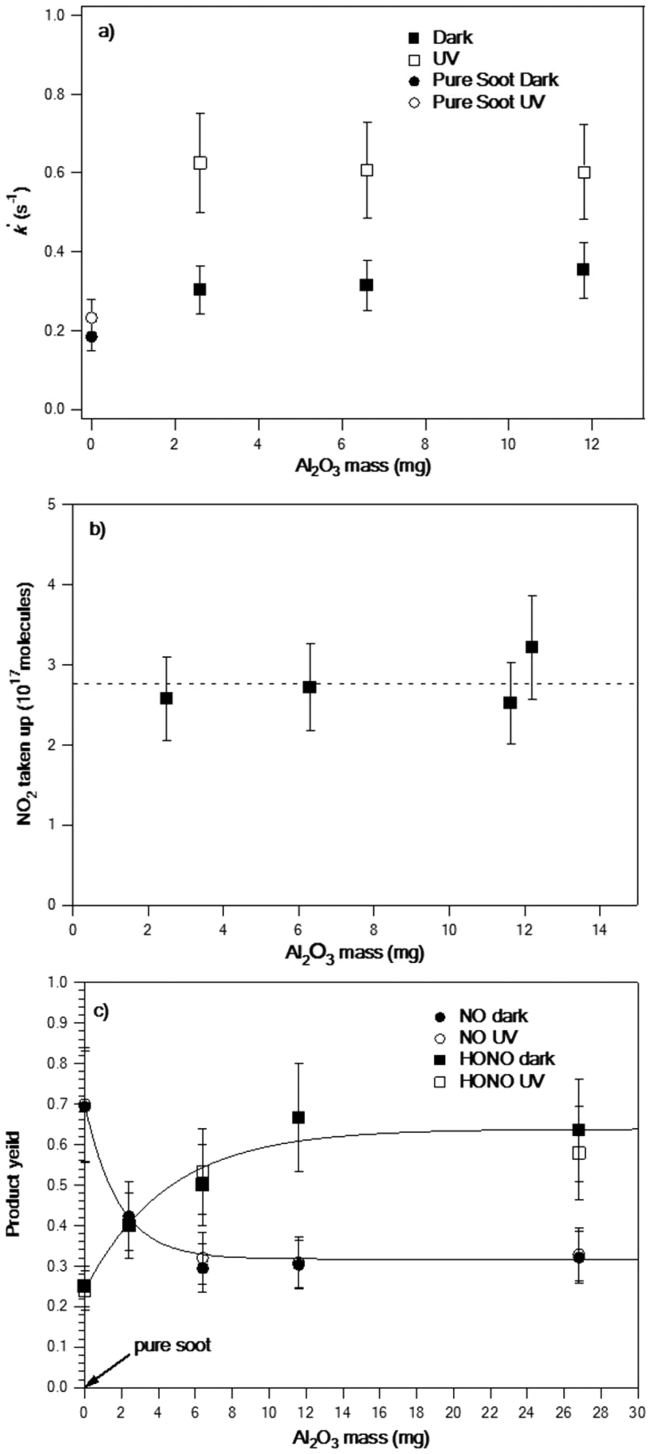

Figure 3. Effects of the Al_2O_3/soot sample composition on the NO_2 uptake and reaction products. Conditions: soot mass = 2 mg, T = 293 K, RH = 5%, $[NO_2]_0 \approx 2 \times 10^{12}$ molecules cm^{-3}. Solid and open symbols denote experiments under dark and irradiation (J_{NO_2} = 0.012 s^{-1}) conditions, respectively. (a) NO_2 loss rate as a function of mass of Al_2O_3 (circles represent data obtained with pure soot), (b) number of NO_2 molecules lost on the surface versus mass of Al_2O_3 (dashed line represents mean of four measurements), and (c) product yield as a function of Al_2O_3 mass content (solid lines are drawn to guide the eyes and have no physical meaning). For comparison purposes, the product yield on pure soot is noted at zero Al_2O_3 mass.

dx.doi.org/10.1021/jp407914f | J. Phys. Chem. A 2013, 117, 12897−12911

results are presented in Figure 4 as k'_{UV}/k'_{dark} (NO_2 uptake enhancement upon irradiation) versus soot mass. We found

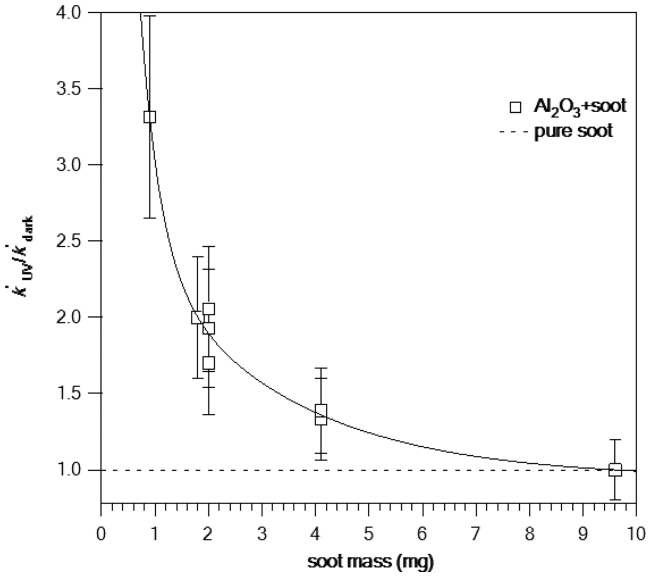

Figure 4. Plot of k'_{UV}/k'_{dark} versus soot mass. Experiments performed at T = 293 K, 5% RH, and $[NO_2] \approx 2 \times 10^{12}$ molecules cm^{-3}. Open squares denote results on 11.6 mg of Al_2O_3 covered with different masses of soot. The dashed line corresponds to the k'_{UV}/k'_{dark} ratio on pure soot, where no effect from UV light was observed. The solid line is the exponential fit of the results on Al_2O_3/soot surfaces.

that the impact of UV irradiation decreased exponentially with increasing soot coverage thickness. In particular, the ratio k'_{UV}/k'_{dark} asymptotically approached 1 (dashed line), corresponding to the absence of a UV effect as observed on pure soot when the soot mass exceeded 9.5 mg; that is for a soot weight content, defined as soot mass/(soot + Al_2O_3) mass, of >80%. The maximum UV enhancement of NO_2 uptake was observed at the lowest soot mass used in these experiments (factor of 3.3 at m = 0.9 mg). The $\gamma_{ss,BET}$ values measured in this case were higher than those on pure soot by factors ~2 and ~6.6 under dark and UV irradiation conditions, respectively. Unfortunately, it was impossible to perform experiments at lower soot masses, because the soot coverage was not homogeneous, at least to the eye. The data in Figure 4 indicate a masking effect of soot on Al_2O_3, leading to the dependence of the measured uptake coefficient on the mixed sample composition. It is clear that the procedure of sample preparation used in the present work, although allowing for the qualitative study of NO_2 uptake, prevented quantitative measurements. To carry out more thorough measurements of the uptake coefficient, homogeneously mixed soot/mineral oxide samples are needed. For comparison purposes, the experiments on Al_2O_3 + soot surfaces described below were performed with a fixed mass of soot of 2 mg.

3.3.3. Concentration Dependence. A series of experiments was performed in which the uptake coefficient was studied as a function of the initial concentration of NO_2. These experiments were performed under dark and UV irradiation conditions at 293 K and 5% relative humidity, with the initial NO_2 concentration ($[NO_2]_0$) varied in the range of (0.2−10) × 10^{12} molecules cm^{-3}. The results are summarized in Figure 5a, where solid and open symbols denote experiments under dark conditions and in the presence of UV irradiation (J_{NO_2} = 0.012

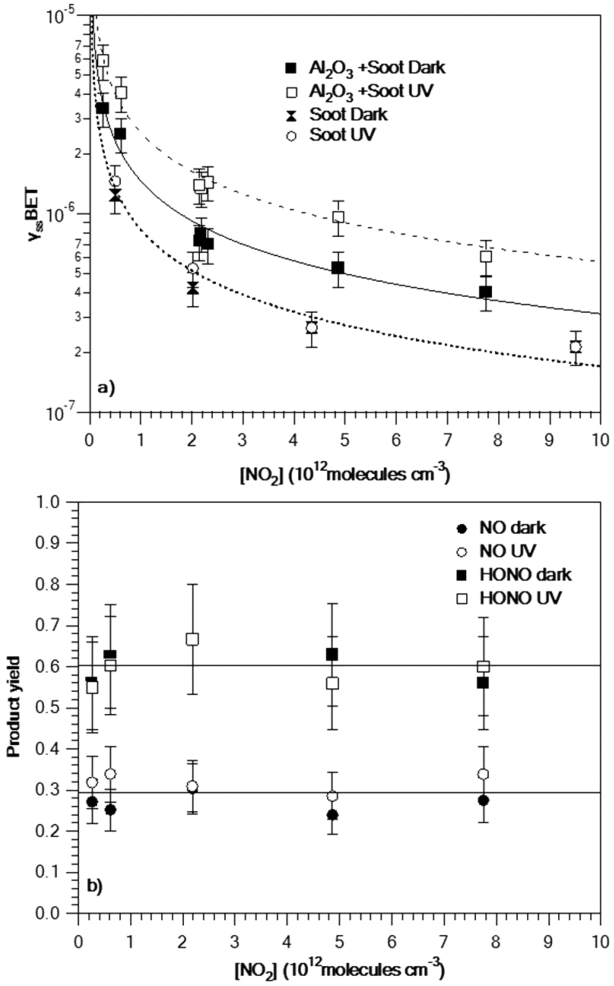

Figure 5. Influence of the NO_2 initial concentration on the uptake coefficient and the product yield for uptake on 11.6 mg of Al_2O_3 covered with 2 mg of kerosene soot. Experiments were conducted at T = 293 K, 5% RH, and 9 Torr total pressure. Solid and open points represent results obtained under dark and UV light irradiation (J_{NO_2} = 0.012 s^{-1}) conditions, respectively. (a) Uptake coefficient measurement. For comparison purposes, $\gamma_{ss,BET}$ on pure soot is also presented. Solid, dashed, and dotted lines correspond to fits of the experimental results using an empirical power function of the form $Y = 10^a[NO]_2^b$. (b) Distribution of gas-phase products. The yield of HONO formation was determined to be (60 ± 12)% (squares), whereas the NO yield was (30 ± 6)% (cycles). Solid lines express the means of the yields in the overall concentration range. Error bars express the overall uncertainty in the yield determination.

s^{-1}), respectively. The $\gamma_{ss,dark}$ and $\gamma_{ss,6UV}$ values for pure kerosene soot surfaces are also included. In all cases, an inverse dependence of the uptake was observed, which can be attributed to surface saturation by the adsorbed precursor and depletion of photoproduced intermediates in the presence of UV irradiation. Over the whole concentration range studied, the uptake of NO_2 on Al_2O_3 coated with soot was found to be a factor of 2 higher under UV light irradiation than under dark conditions. Concerning pure soot surfaces, we did not observe a clear enhancement of γ_{ss} by UV light. The dependence of γ_{ss} on the concentration of NO_2 can be parametrized with the following empirical expressions: $\gamma_{ss,6UV} = 10^{2.2} \times [NO_2]_0^{-0.65}$ and $\gamma_{ss,dark} = 10^{2.2} \times [NO_2]_0^{-0.67}$ for Al_2O_3 surfaces covered with soot and $\gamma_{ss} = 10^{2.2} \times [NO_2]_0^{-0.69}$ for pure soot under dark and

dx.doi.org/10.1021/jp407914f | J. Phys. Chem. A 2013, 117, 12897−12911

UV irradiation conditions, with $[NO_2]_0$ in units of molecules cm^{-3}.

In addition to the kinetics, the yield of the gas-phase products was examined in the same range of initial NO_2 concentrations ($[NO_2]_0$), and the results are shown in Figure 5b. Solid and open points denote experiments under dark and UV light irradiation conditions, respectively. The yields of HONO and NO were nearly 60% and 30%, respectively, independent of the initial NO_2 concentration and irradiation conditions. For pure soot surfaces, not included in the figure, the yield was also independent of NO_2 concentration; however, the distribution of the gas-phase products was different, with yields of approximately 20% and 60−70% for HONO and NO, respectively.

Finally, it should be noted that, for comparison purposes, the measurements of the uptake coefficient and product yield under different experimental conditions presented below were carried out at a fixed NO_2 concentration of $\sim 2 \times 10^{12}$ molecules cm^{-3}. This value was the result of a compromise between the need to work with low concentrations relevant to the atmosphere and the NO_2 detection limit.

3.3.4. Dependence on Irradiance Intensity. The objective of the current series of experiments was to determine the $\gamma_{ss,BET}$ value of NO_2 and product yield as functions of the UV irradiance intensity. The mixed mineral/organic aerosol surfaces, ~11.6 mg of Al_2O_3 covered with 2 mg of soot, were exposed to 2×10^{12} molecules cm^{-3} of gaseous NO_2 at T = 293 K and RH = 5%. The light source was characterized by directly measuring the photolysis frequency of NO_2, J_{NO_2}, inside the flow reactor.[12] The values obtained were 0.002 and 0.012 s^{-1}, respectively, for one and six UV lamps switched on, corresponding to J_{NO_2} values in the atmosphere under cloudy and clear sky conditions, respectively.[14] The experimental results showed a linear relationship between $\gamma_{ss,BET}$ and irradiance intensity, pointing to the photocatalytic nature of the heterogeneous reaction (Figure 6a). The intercept of the straight line corresponds to the value of γ_{ss} measured under dark conditions. In addition, the distribution of the gas-phase products was found to be independent of the irradiance intensity (Figure 6b). Approximately 60% HONO (squares) and ~30% NO (cycles) were formed, leading to a nitrogen mass balance of ~90%. The solid lines correspond to the mean values obtained for the product yield.

3.3.5. Dependence on Relative Humidity (RH). It has been established that water molecules can influence the reaction rates and product yields of heterogeneous reactions.[15] In particular, H_2O can either reduce the reaction rate, by blocking available surface sites,[11b] or enhance the reaction, by creating reactive species on the surface.[11a] The effects of RH on the uptake and product distribution were examined over a wide range, (RH = 0.0032−32%). It should be noted that, under the current experimental operating conditions, T = 293 K and P = 9−10 Torr, higher levels of relative humidity could not be achieved in our low-pressure flow reactor. The experiments were performed under dark and UV light irradiation conditions, using a NO_2 concentration of $\sim 2 \times 10^{12}$ molecules cm^{-3} and a soot mass of 2 mg. The results are summarized in Figure 7. Concerning the uptake process in the dark, $\gamma_{ss,BET}$ was found to be almost independent of RH between 0.0032% and 5%, whereas for the same range of RH in the presence of UV light irradiation, a slight decrease of the uptake coefficient was observed. However, the further increase of RH to 30% was found to

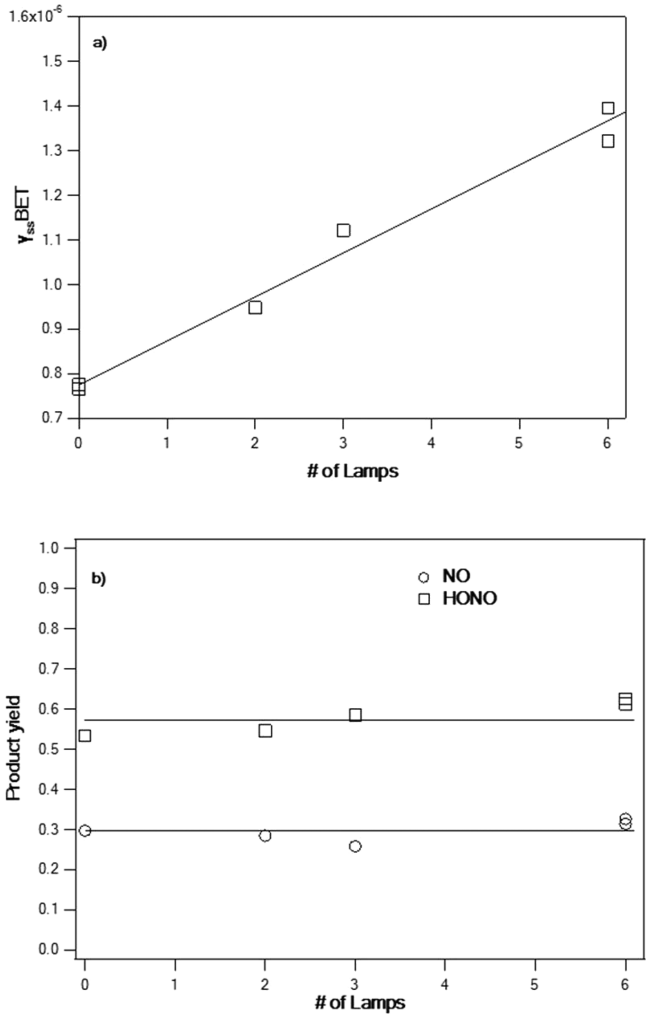

Figure 6. Impact of UV irradiance intensity on the (a) uptake coefficient and (b) distribution of products. Experiments were performed at T = 293 K and RH ≈ 5%, exposing 11.6 mg of Al_2O_3 covered with 2 mg of kerosene soot to $[NO_2] \approx 2 \times 10^{12}$ molecules cm^{-3}.

enhance $\gamma_{ss,BET}$ in both cases. Attempting to parametrize the dependence of $\gamma_{ss,BET}$ over the entire RH range studied, shown by the solid and dashed lines in Figure 7a, the following expressions were obtained

$$\gamma_{ss,BET,dark} = (7.3 \pm 0.9) \times 10^{-7} + (3.2 \pm 0.5) \times 10^{-8} \times RH$$

$$\gamma_{ss,BET,UV} = (1.4 \pm 0.2) \times 10^{-6} + (4.0 \pm 0.9) \times 10^{-8} \times RH$$

It should be noted that the parametrization fails to fit the data for dry conditions (RH ≤ 0.1%) in the presence of UV irradiation; however, the results at RHs relevant to the atmosphere are well-fitted.

The effects of water on the distribution of reaction products are shown in Figure 7b, where squares and cycles indicate HONO and NO yields, respectively. Solid and open points represent the results observed under dark and UV light irradiation conditions, respectively. Dashed and solid lines were drawn just for indication and have no physical meaning. HONO yield was found to increase with RH, reaching a steady

dx.doi.org/10.1021/jp407914f | J. Phys. Chem. A 2013, 117, 12897−12911

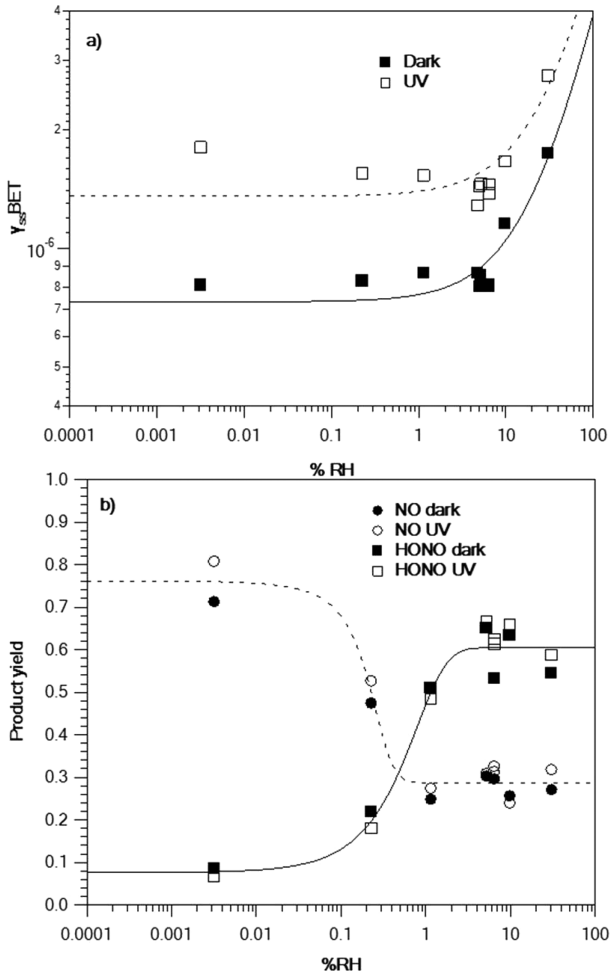

Figure 7. Impact of relative humidity on the uptake coefficient and reaction products. Experiments were conducted at T = 293 K with relative humidities in the range of 0.0032−32%. In each experiment, 11.6 mg of Al_2O_3 covered with 2 mg of soot was exposed to a NO_2 concentration of ∼2 × 10^{12} molecules cm^{-3}. Solid and open points denote experiments under dark and UV irradiation conditions, respectively. (a) Solid and dashed lines are linear fits of the experimental results under dark and UV light irradiation conditions, respectively. (b) Solid and dashed lines indicate the impact of RH on the branching ratios of NO and HONO, respectively. Lines were drawn to guide the eyes and have no physical meaning.

value of ∼60% at RH ≈ 4%. On the contrary, the NO yield decreased with RH, reaching a minimum value at RH ≈ 1%. This is a clear indication that H_2O participates in the reaction scheme in a manner that favors HONO production.

3.4. Effect of Sample Heating. Soot particles formed from the incomplete combustion of hydrocarbon fuels contain a variety of semivolatile compounds such as PAHs, alcohols, carboxylic acids, and saturated and unsaturated hydrocarbons.[1a,c] To investigate the potential effects of these compounds on the uptake process, a series of experiments was performed with surfaces of pure soot and Al_2O_3 covered with soot heated prior to their exposure to NO_2. After preparation, the samples were placed inside an exhaust ventilation chamber and heated for 3.5 h at T = 350 °C. This method was preferable to heating inside the reactor under pumping, to avoid condensation of the desorbed compounds on the reactor walls, which would contaminate the system. It should be noted that, at these temperatures, the major fraction of volatile compounds and PAHs adsorbed on the surface are removed.[10a,16] The uptake and product data obtained with preheated samples are summarized in Figure 8 and Table 1. Concerning the pure

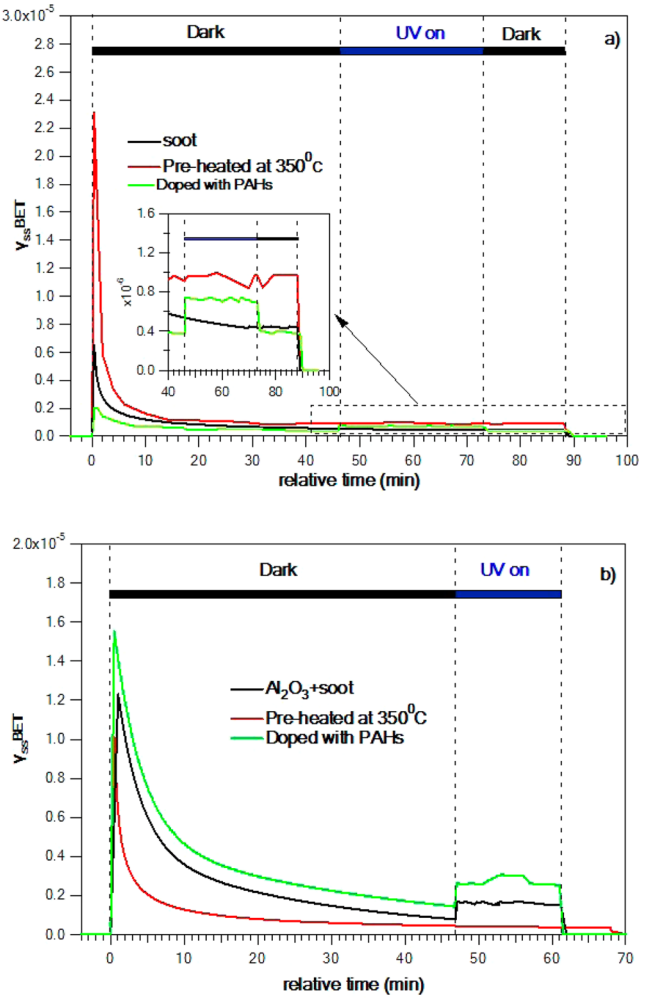

Figure 8. Time-dependent profiles of γ_{ss} for (a) pure soot and (b) soot/Al_2O_3 surfaces, obtained upon different sample treatments. Experiments were performed at T = 293 K and ∼5% RH using [NO_2] ≈ 2 × 10^{12} molecules cm^{-3} in the presence and absence of UV light. Black, red, and green lines denote experiments with undoped surfaces, surfaces heated to 350 °C, and surfaces doped with PAHs, respectively.

soot surface (Figure 8a), the reactivity toward NO_2 was enhanced after heating. The number of NO_2 molecules taken up/reacted during 45 min of exposure was approximately 2 times higher on a preheated surface. The initial and steady-state uptake coefficients were increased by factors of 4 and 2, respectively, and no effect of UV light was observed. Apparently, the semivolatile compounds act as inhibitors of NO_2 uptake, occupying active surface sites. Heating removes these compounds from the surface, liberating the active sites, and results in an enhanced reactivity. This is also an indication that the reaction of NO_2 with soot is faster than that with reversibly adsorbed semivolatile compounds, such as PAHs, in agreement with the findings of Nguyen et al.[17] The preheating of the soot sample also had an impact on the product distribution. The HONO yield increased from 20% to 53%, whereas the NO yield decreased from 70% to 32%. This finding is in accordance with the work of Khalizov et al., who observed that the HONO yield increased by a factor of ∼2 upon the

dx.doi.org/10.1021/jp407914f | J. Phys. Chem. A 2013, 117, 12897−12911

heating of kerosene soot at 300 °C.[9w] They also observed an increase in NO_2 reactivity that they attributed to the desorption of incomplete combustion products, liberating reactive sites. However, it should be noted that the enhancement in soot reactivity observed in our experiments upon thermal treatment in air could be also due to a change in the chemical composition of the soot samples through the transformation of the functional groups on the surface.

On the contrary, heating caused a decrease of the uptake coefficient on Al_2O_3 covered with soot (Figure 8b). The number of molecules taken up in the first 45 min of exposure was one-half that on the unheated surface and close to the number of molecules measured on pure soot surfaces. Furthermore, the effect of UV light was extinguished (t = 47 min in Figure 8b). The later observation suggests that a fraction of the removed semivolatile compounds contains reactive chromophore species that accelerate the reaction under UV irradiation. Thus, it seems that this fraction of molecules inhibits the reaction on pure soot, whereas on soot-covered Al_2O_3 surfaces, it accelerates the reaction under UV irradiation. Regarding the products, the HONO yield was diminished, from 60% to 20%, whereas the NO formation was constant, ∼30%. This also differs from the results obtained with pure soot, for which the HONO yield was increased after heating. In conclusion, this series of experiments revealed the combined effects of Al_2O_3 and semivolatile compounds on the chemical reactivity of mixed Al_2O_3/soot samples. The presence of Al_2O_3 is necessary to activate a fraction of molecules that remain inactive or have lower reactivity in pure soot.

3.5. Effect of PAH Doping. The role of organic compounds and particularly of PAHs in heterogeneous chemistry is still under investigation, although their potential significance has been stressed over the past decade.[6b,17,18] Recent studies have shown that, on solid PAH surfaces or substrates containing PAH molecules, UV light can enhance the reaction rate significantly.[9x−z,18b,19] The objective of the current series of experiments was to investigate the role of PAHs in pure soot and soot-doped Al_2O_3 surfaces. To this end, 15 different PAH compounds (Table S1, Supporting Information) were used to dope the substrates. Experiments were performed at temperature (T) of 293 K, a relative humidity (RH) of 5% , and a NO_2 concentration ($[NO_2]$) of $\sim 2 \times 10^{12}$ molecules cm^{-3}. The results are displayed in Figure 8 and Table 1.

For pure soot surfaces, the initial uptake coefficient was found to decrease significantly after doping (green line, Figure 8a), with the steady-state uptake being close to that on untreated soot. This observation is in agreement with heating experiments from which we concluded that desorption of semivolatile compounds, including PAHs, increases the uptake coefficient. On the contrary, irradiation of PAH-doped soot increased the uptake coefficient by a factor of 2 compared with that of nondoped soot, showing that the effect of UV irradiation on soot reactivity depends on the amount and/or identity of the surface PAHs. Concerning the products, the HONO yield increased from 20% on pure soot to 43% on soot-doped Al_2O_3, whereas NO was reduced from 70% to 38% and 53% in the dark and under UV light, respectively.

PAH doping of the Al_2O_3 surface covered with soot caused an increase in the uptake coefficient, as can be seen in Figure 8b (green line). This enhancement was observed even under dark conditions. Moreover, as expected, UV irradiation of the reactive surface led to a substantial increase in the NO_2 uptake (see also Table 1). The yield of HONO decreased slightly after doping and was independent of irradiation conditions. Conversely, irradiation of the surface increased the NO yield from 17% (under dark) to 43%. The yield of the reaction products seems to be a complex function of the state of the reactive surface (heating, doping, ±UV), with a probable impact of secondary HONO chemistry.

The experiments with sample preheating and PAH doping seem to clearly show that Al_2O_3 promotes the activation of chromophore species hosted on soot. In this respect, a question arises as to the effect of the presence of PAHs on the surface of mineral aerosol on its reactivity. We performed qualitative experiments in which pure Al_2O_3 doped with PAHs was exposed to NO_2. A very strong effect of UV irradiation was observed: The uptake coefficient of NO_2 increased by almost 2 orders of magnitude when on the light was switched on. This seems to be strong evidence that the reactivity of a mineral aerosol can be dramatically changed in the presence of UV-absorbing organics on its surface, which should be addressed in future studies.

3.6. UV−Vis−NIR Study of Solid Samples. The absorption spectra of eight solid substrates were studied to determine the effects of different applied treatments to the optical properties of the surfaces. Results are presented in Figure S3 (Supporting Information). Although equal masses of solids were used, the differences in the BET surface areas could affect the intensity of the absorbance. Soot spectra displayed a broad absorption band in the entire UV−vis−NIR range. Similar spectra were also recorded earlier.[20] The existence of Al_2O_3 on soot caused a significant increase of the absorption efficiency of the solid (lines 6 and 7). Treatment of pure and soot-doped solid Al_2O_3 surfaces with NO_2 for 1 h, lines 3 and 7, respectively, also increased the absorption capability. This can be attributed to the formation of nitro-PAHs or other oxidation compounds. Indeed, comparing the UV spectra of nitro-PAHs formed with the corresponding PAHs precursor, the absorbance maxima are increased in the blue range, and a red shift to the spectrum was also observed.[21] Heating of pure soot at 350 °C for 3.5 h in a laboratory environment also amplified the absorption. Probably, the thermal decomposition of low-volatility organic compounds on soot or their oxidation by atmospheric oxygen forms surface products with stronger absorption capacities. Finally, on PAH-doped surfaces, enhancement of the absorption patterns was recorded. The doped Al_2O_3 surfaces showed a sharp band between 200 and 400 nm.

3.7. Comparison with Previous Studies. To our knowledge, there are no existing experimental data for the reaction of NO_2 with soot-covered Al_2O_3 for comparison with our results. The only comparison that can be made concerns pure soot. In particular, under dark conditions, the heterogeneous interaction of soot with NO_2 has been extensively studied, and the results are well summarized and compared in the publications of Aubin and Abbatt[9t] and Lelievre et al.[9ab] The scattering of the data presented therein can be attributed to the different experimental conditions. A detailed comparison of our results with the existing data is not presented herein because it is beyond the scope of the present study. Instead, we confine ourselves to the conclusion that both the uptake coefficient and the product yield determined here are in agreement with the majority of the already-published experimental results and present only a brief summary.

The published data showed a strong decrease of γ with increasing NO_2 concentration, similar to what we observed

here. In addition, soot surfaces produced under fuel-rich flame conditions exhibited higher uptake coefficients, by a factor of 2−10, than under fuel-lean flame conditions.[9m,p,v,w] An average value of γ_0 of $(2-5) \times 10^{-5}$ has been measured at NO_2 concentrations of $\sim 10^{11}$ molecules cm^{-3} for all kind of fuels. γ_{ss} was a factor of 5−10 lower than γ_0, in agreement with our results, where, for similar concentrations, γ_{ss} was $\sim 10^{-6}$. Regarding the products, HONO and NO have been reported as the sole nitrogen-containing compounds, whereas no N_2O or HNO_3 have been observed in the gas phase; however, the formation of surface-adsorbed HNO_3 cannot be excluded. The yields of NO and HONO reported in different studies range from 10% to 100%.[9m,p,w,22] Aubin and Abbatt reported that the HONO yield decreased at lower temperatures, probably because of HONO remaining adsorbed on the soot surface after being formed.[9t] Similar behavior was observed by Longfellow et al.,[9i] who reported low yields, between 10% and 30%, on methane, propane, kerosene, and hexane soot at 262 K. Gerecke et al.[22] found that the HONO yield decreased with increasing distance from the flame base, whereas the inverse was observed for NO. Rossi and co-workers[9k,m] showed 70−100% conversions of NO_2 to HONO when the NO_2 was adsorbed and reacted on rich decane soot surfaces where no NO production was observed. It has been proposed that the low HONO yields determined imply not that HONO is not being produced but rather that it is rapidly decomposed on the soot surface, yielding NO. This statement was confirmed in reference uptake experiments in which HONO interacting with toluene and decane soot led to 5−25% losses, whereas 90% of the HONO reacted with acetylene soot.[9k] Likewise, HONO was found to decompose on decane soot formed under lean flames, whereas no decomposition was recorded on decane soot produced under rich flame conditions.[9p] In conclusion, these observations could imply that HONO is produced in high yields on all types of soot but decomposes on some surfaces, reducing the observed yield.

In the present study, we did not observe any enhancement of the NO_2 uptake on pure soot in the presence of UV light. In contrast, Monge et al.[9x] detected a substantial increase, approximately 1 order of magnitude, of the uptake coefficient upon irradiation of a soot surface. In that study, propane was used as the fuel to produce soot particles under different richness conditions. Experiments were performed using a flow-tube reactor at 298 K under atmospheric pressure and a relative humidity of 30%. The values of the uptake coefficient were determined to be between 2×10^{-8} and 2×10^{-7} for dark and irradiation conditions, respectively, for a NO_2 concentration of $\sim 6.25 \times 10^{11}$ molecules cm^{-3}. Han et al. reported an enhancement of the soot aging process by NO_2 in the presence of simulated sunlight; however, the uptake coefficient was not measured.[9z] Actually, our data on the absence of a UV effect and those reported by Monge et al.[9x] on the enhancement of the NO_2 uptake on a soot surface in the presence of UV irradiation do not contradict each other. The reactivity of soot depends on its origin (fuel) and combustion conditions. The soot samples used in our study and that of Monge et al. were different, and this could be the reason for the differing uptake coefficients measured in two studies. The uptake coefficient measured in this work under dark conditions ($\gamma_{ss} \approx 4 \times 10^{-7}$, Table 1) is an order of magnitude higher than that measured by Monge at al. ($\gamma_{ss} \approx 4 \times 10^{-8}$ for asimilar NO_2 mixing ratio of 80 ppb) in the presence of UV irradiation. This suggests that, in our measurements, the probable relatively low contribution of photoinitiated uptake could just be hidden by the rapid dark reaction.

3.8. Role of Al_2O_3 in Reactivity. In this section, we attempt to clarify the role of Al_2O_3 in the chemical system studied. Summarizing the results, we observed that, on soot-covered Al_2O_3 surfaces, γ_{ss} is increased, compared with that on pure soot, but it is independent of the Al_2O_3 mass used. The uptake was substantially enhanced under UV light irradiation, a phenomenon observed with neither pure soot nor pure Al_2O_3 surfaces. Regarding the reference heating and PAH doping experiments, we showed that Al_2O_3 promotes the activation of chromophore species hosted on soot. Concerning the products, their distribution was also influenced, with HONO formation being favored in the presence of Al_2O_3.

Before we begin with the interpretation of the results, let us make a quick "tour" of materials science where similar phenomena have been observed and helpful conclusions presented. The improvement of organic solar cells, also known as photovoltaic cells, is a new domain of materials science aimed at generating power from solar light.[23] Organic polycyclic polymer compounds are used as absorbents instead of high-cost inorganic compounds. Recent studies have shown that a thin film of Al_2O_3 can improve the efficiency of these organic cells.[24] Briefly, the organic compounds contain molecular $\pi-\pi^*$ orbitals corresponding to the highest occupied molecular orbital (HOMO) and lowest unoccupied molecular orbital (LUMO).[25] For simplicity, such organic materials can be regarded as semiconductor-like materials, where the band gap corresponds to the difference between the LUMO and HOMO. When a photon with sufficient energy is incident on the organic semiconductor, it can be absorbed to produce an excited state. The lifetime of the excitation is crucial. To produce photocurrent, the electron−hole pair must be separated. If not, a recombination process takes place. Therefore, after light absorption, the carriers should be separated and finally collected from the anode and cathode. The utility of Al_2O_3 arises at this step. A thin film of Al_2O_3 deposited on the cathode of the cell acts as an electron acceptor, collecting the electrons and increasing the efficiency of the photovoltaic system.[24−26] In addition, alumina in combination with other compounds is used as a separator material to separate the electrons formed, preventing the recombination process and extending the lifetime of the excitation.

Returning to our experiments, the previous discussion can be used to interpret the results. In particular, regarding the soot-covered Al_2O_3 surfaces, the acceleration of the reaction in the presence of UV light can be attributed to the efficiency of Al_2O_3 as an electron acceptor. Initially, light excites the chromophore compounds hosted on soot, such as PAHs, and Al_2O_3 traps the electrons, preventing the recombination process and extending the lifetime of the excitation. Subsequently, a sequence of electrochemical reactions can be initiated in which adsorbed NO_2 can participate, resulting in its gas-phase consumption. Therefore, the difference with pure soot lies in the lifetime of the excited states of the organics. On pure soot, the recombination process is faster, downgrading the significance of light and of the organics. Furthermore, the fact that γ_{ss} was found to be independent of the Al_2O_3 mass possibly indicates that the charge transfer is localized at the Al_2O_3/soot interface; thus, only a thin film is required. The former possibility is supported by the results presented in Figure 4, where the

Scheme 1

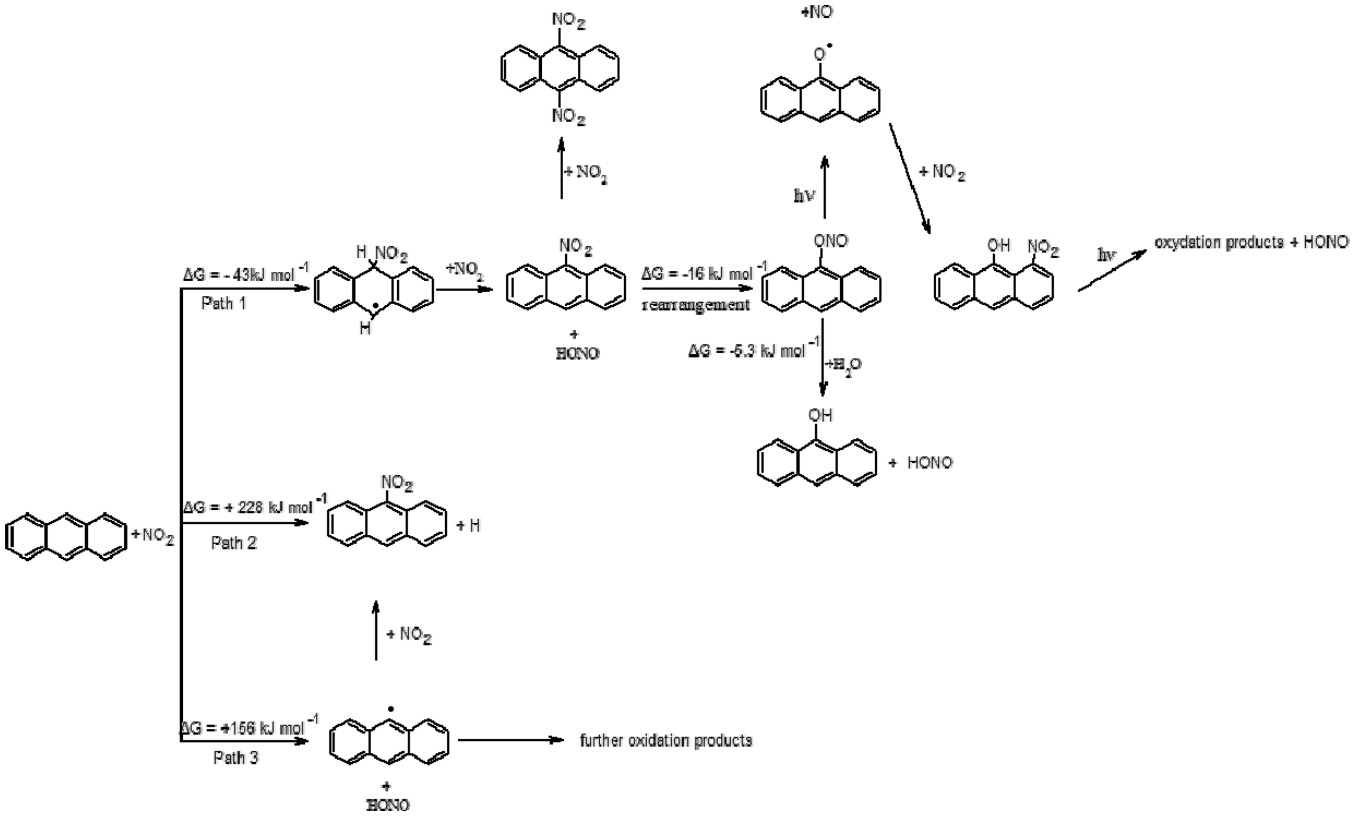

impact of UV irradiation was more pronounced on samples with lower soot weight contents.

Under dark conditions, it is difficult to identify the role of Al_2O_3 in acceleration of the heterogeneous reaction because there is no light to induce electron production. A possible explanation could be the inception of a sequence of redox reactions even in the dark. This can be attributed to the special properties of Al_2O_3, which can contain a very high density of negative charges, up to 10^{13} cm^{-2}, and also behaves as an effective hydrogen reservoir.[24a] In the presence of organic molecules, the redox reactions might be promoted and lead to NO_2 consumption. Indeed, electron paramagnetic resonance (EPR) studies in the absence of light have shown that adsorption of anthraquinone and *o*-chloranil on Al_2O_3 initiates electron-transfer processes, producing free radicals at the active sites of alumina.[27]

3.9. Reaction Mechanism. The interaction of NO_2 with different types of soot under dark conditions has been intensively studied, and several reaction pathways have been proposed.[9h,i,22,28] In particular, the following reduction−oxidation reactions were proposed to interpret the reaction products, NO and HONO, observed in the gas phase

$$\{SS\} + NO_2(g) \leftrightarrow \{SS{-}NO_2\} \quad (3)$$

$$\{SS{-}NO_2\} \rightarrow \{SS{-}O\} + NO(g) \quad (4)$$

$$\{SS{-}H\} + NO_2(g) \rightarrow \{SS\} + HONO(g) \quad (5)$$

where the braces denote surface-bound species and {SS} represents different active sites or functional groups on the soot surface. Kleffmann et al.[9h] observed that HONO formation is favored under humid conditions and proposed the following reactions

$$\{SS{-}NO_2\} + \{SS{-}H_2O\} + \{SS\}_{red} \rightarrow \{SS{-}HONO\} + \{SS\}_{ox} \quad (6)$$

$$\{SS{-}HONO\} \leftrightarrow HONO(g) \quad (7)$$

where $\{SS\}_{red}$ and $\{SS\}_{ox}$ represent reduced and oxidized surface sites, respectively. Recall that an increase in the HONO yield at elevated RH (Figure 7b) was also observed for NO_2 uptake on the mixed soot/Al_2O_3 surface in the present study. A few studies have reported the decomposition of HONO on soot surfaces, leading to NO_2 and NO as final reaction products.[9h,k]

It is generally believed that the reactivity of soot is determined by its organic fraction, present on the surface in the form of surface-adsorbed and/or -bound species and functional groups. PAHs comprise a fraction of these compounds (see Table S1, Supporting Information), and because nitro-PAHs were detected as reaction products, we decided to use anthracene as a reference molecule to propose a reaction scheme. In combination with our observations, DFT calculations were conducted to specify the possible favorable channels leading to the final products. All of the corresponding conformer structures were obtained by performing geometry optimization calculations at the B3LYP/6-31G(d) level of theory with the Gaussian 09 program suite.[29] Thermochemical parameters were taken from the vibrational frequency calculations at the same level of theory.

The reaction of NO_2 with anthracene can proceed through three different pathways, as displayed in Scheme 1. For brevity, the mechanism described therein represents dark and UV irradiation conditions, and the only difference concerns the addition of extra pathways upon irradiation of the surface. In

dx.doi.org/10.1021/jp407914f | J. Phys. Chem. A 2013, 117, 12897−12911

the first path, two NO_2 molecules attack anthracene in two steps, forming as final products nitroanthracene and HONO. The Gibbs free energy for the double step addition of NO_2 is $\Delta G = -43$ kJ mol^{-1}. The first NO_2 molecule is added to the ring and forms an adduct, whereas the second NO_2 can either abstract one H atom or be added to the carbon ring, producing a complex that will further decompose to give the final products.[30] Paths 2 and 3 represent the direct NO_2 addition and H abstraction from anthracene, respectively. According to our calculations, these steps are not spontaneous, as $\Delta G = +228$ kJ mol^{-1} for the direct addition and $\Delta G = +156$ kJ mol^{-1} for the abstraction, so they are unlikely to occur under dark conditions. However, in the case of surface irradiation with UV light, the absorbing PAH molecules are led to an excited state. A rough estimation of the energy supplied to the reaction system gives ~299−380 kJ mol^{-1}, which is sufficient to exceed the required energy content of paths 2 and 3. Therefore, from a thermodynamic perspective, the reaction is expected to proceed through pathways 2 and 3 as well under UV irradiation.

The formed 9-nitroanthracene can further react with NO_2, producing 9,10-dinitroanthracene,[31] or undergo a rearrangement of the nitro group, giving nitrite anthracene, R−ONO, $\Delta G = -16$ kJ mol^{-1}. Then, in the presence of light, nitrite anthracene can be photolyzed, giving an RO-type radical that can subsequently react with NO_2 to produce nitrophenols.[32] Alternatively, nitrite anthracene can form a stable complex with H_2O, producing hydroxyanthracene and HONO. The former pathway is favorable thermodynamically because $\Delta G = -5.3$ kJ mol^{-1}. Thereafter, the classic mechanism of phenol nitration can take place to produce nitrophenols.

Regarding the mixed Al_2O_3/soot substrates, an additional set of reactions can occur on the surface. A tentative simplified mechanism based on our experimental observations and literature data is proposed in the following equations. Al_2O_3 acts as an electron acceptor, initiating a number of electrochemical surface reactions that consume NO_2. The excitation of organics with UV light can switch on the electron-transfer mechanism, leading to alumina reduction and PAH oxidation according to reaction 8. PAH^+ can be reduced in reaction with water 9, forming OH radicals.[33]

$$Al^{3+}{-}PAH + h\nu \leftrightarrow Al^{2+}{-}PAH^+ \quad (8)$$

$$PAH^+ + H_2O \rightarrow H^+ + {}^{\bullet}OH + PAH \quad (9)$$

Activated in such a way, the reactive system leads to a series of redox reactions similar to those in semiconductor photocatalysis. In particular, HONO and NO detected as the reaction products in the gas phase can be formed in the following processes

$$Al^{2+} + NO_2 \rightarrow Al^{3+} + NO_2^- \quad (10)$$

$$NO_2^- + H^+ \rightarrow HONO \quad (11)$$

$$NO_2^- + h\nu \rightarrow NO + O^- \quad (12)$$

$$NO_2 + O^- \rightarrow NO + O_2^- \quad (13)$$

In addition, NO_2^- can react with excited PAHs to form a nitro-PAH radical, leading to reaction Scheme 1.[30] The OH radicals formed in reaction 9 can undergo recombination or react with the surface PAHs, oxidizing them.[33] Reactions 11−13 seem to explain well the observed dependence of the HONO and NO yields on relative humidity: An increase of HONO (more H^+) and decrease of NO yield with increasing RH (Figure 7b). It should be noted that HONO can be transformed into NO_2 and NO in secondary reactions[11c]

$$HONO + Al^{3+} \rightarrow NO_2 + H^+ + Al^{2+} \quad (14)$$

$$HONO + H^+ + Al^{2+} \rightarrow NO + H_2O + Al^{3+} \quad (15)$$

The interaction of HONO with mixed Al_2O_3/soot surfaces was not tested in the present study. However, the reaction of HONO with pure Al_2O_3 under dark and UV irradiation conditions was investigated in a previous study by our group.[11c] In particular, a rather strong inverse dependence on relative humidity was found for the uptake coefficient of HONO on the Al_2O_3 surface: $\gamma \approx [RH]^{-0.61}$ and $[RH]^{-0.44}$ under dark and UV irradiation conditions. This observation seems to be in line with the increase in the uptake coefficient of NO_2 (Figure 7a) and the increase in the HONO yield at higher RH observed in the present study on mixed soot/Al_2O_3 samples.

In conclusion, it is clear that the simplified mechanism presented above is not complete; however, it qualitatively explains the experimental observations through a series of redox reactions that would not occur in the absence of a photosensitizer.

4. CONCLUSIONS

The aim of the current study was to investigate the chemical reactivity of mixed aerosol surfaces and to reveal their potential role in heterogeneous chemistry. To this end, the interaction of Al_2O_3 surfaces covered with kerosene soot with NO_2 was investigated at 293 K under different experimental conditions. The results showed that $\gamma_{ss,BET}$ was approximately 2−6.6 times higher than the sum of γ_{ss} values on individual surfaces, under dark and UV irradiation conditions, respectively. An increase of $\gamma_{ss,BET}$ with relative humidity and irradiance intensity was observed. In addition, Al_2O_3 was found to favor the formation of HONO. The yield of HONO increased from 20% on pure soot to 60% on Al_2O_3/soot surfaces. Experiments with surface preheating and doping with PAHs showed that PAHs accelerate the uptake on mixed soot/Al_2O_3 surfaces, whereas on pure soot, they substantially inhibit the reaction. The former effect was attributed to the efficiency of Al_2O_3 as an electron acceptor. Chromophore PAH compounds absorb UV light, creating an excited state, from which Al_2O_3 can either collect the electrons or prevent the recombination process, extending the lifetime of the excited state. Consequently, a sequence of redox reactions takes place, leading to the depletion of NO_2. The results of experiments with varying Al_2O_3 and soot masses support the fact that the charge transfer was localized at the Al_2O_3/soot interface; thus, only a thin film of Al_2O_3 is required to accelerate the reaction.

Regarding the atmospheric implications, using $\gamma_{ss} = 2 \times 10^{-6}$ for a NO_2 mixing ratio of 25 ppb, a HONO yield of 60% and an aerosol soot loading of 30 μg m^{-3}, Monge et al.[9x] estimated a HONO formation rate of ~40 pptv h^{-1} under solar irradiance conditions. The present results show that the contribution of the heterogeneous photochemistry of NO_2 on the soot surface to the daytime HONO concentration can be even higher, by at least a factor of 3 (e.g., Figure 5a), if soot is mixed with Al_2O_3 (and possibly with other mineral oxides).

The major finding of the current study is the demonstration that mineral dust can change the atmospheric reactivity of soot and vice versa. The rate of the uptake process and the product yield can be completely different from those on the pure

surfaces. Thus, the mixing and/or covering of aerosols should be viewed not as an additive but as a synergetic effect, especially in the presence of solids containing photosensitizer compounds. Unfortunately, the procedure of sample preparation used in the present study (soot deposited on Al_2O_3 film), is not very suitable for thorough measurements of uptake coefficients. Therefore, new efforts should be made through laboratory studies focusing on homogeneously mixed soot/mineral oxide samples. Another point that merits a detailed study is the reactivity of mineral aerosols covered with UV-absorbing organics, which can be dramatically enhanced under UV irradiation, as shown in the present study.

■ ASSOCIATED CONTENT

Supporting Information

One table with a detailed list of the PAH compounds detected in soot and used for doping experiments. Scheme of the photochemical reactor in which the experiments were performed. Two figures, showing the mass dependence of γ_{ss} on pure soot and the solid state UV−vis−NIR spectra of the substrates used in the current study. This material is available free of charge via the Internet at http://pubs.acs.org.

■ AUTHOR INFORMATION

Corresponding Author

*Tel.: +33 238255474. Fax: +33 238696004. E-mail: manolis.romanias@cnrs-orleans.fr.

Notes

The authors declare no competing financial interest.

■ ACKNOWLEDGMENTS

The research leading to these results received funding from the European Research Council under the European Community's Seventh Framework Programme (FP7/2007-2013)/ERC Grant Agreement 291049-2G-CSafe.

■ REFERENCES

(1) (a) Poschl, U. Atmospheric Aerosols: Composition, Transformation, Climate and Health Effects. *Angew. Chem., Int. Ed.* **2005**, *44* (46), 7520−7540. (b) Daly, H. M.; Horn, A. B. Heterogeneous Chemistry of Toluene, Kerosene and Diesel Soots. *Phys. Chem. Chem. Phys.* **2009**, *11* (7), 1069−1076. (c) Kirchner, U.; Scheer, V.; Vogt, R. FTIR Spectroscopic Investigation of the Mechanism and Kinetics of the Heterogeneous Reactions of NO_2 and HNO_3 with Soot. *J. Phys. Chem. A* **2000**, *104* (39), 8908−8915.

(2) Cooke, W. F.; Wilson, J. J. N. A Global Black Carbon Aerosol Model. *J. Geophys. Res.: Atmos.* **1996**, *101* (D14), 19395−19409.

(3) (a) Satheesh, S. K.; Krishna Moorthy, K. Radiative Effects of Natural Aerosols: A Review. *Atmos. Environ.* **2005**, *39* (11), 2089−2110. (b) Andreae, M. O. Climatic Effects of Changing Atmospheric Aerosol Levels. In *World Survey of Climatology*; Henderson-Sellers, A., Ed.; Elsevier: Amsterdam, 1995; Vol. *16*, Chapter 10, pp 347−398.

(4) Hauglustaine, D. A.; Ridley, B. A.; Solomon, S.; Hess, P. G.; Madronich, S. HNO_3/NO_x Ratio in the Remote Troposphere during MLOPEX 2: Evidence for Nitric Acid Reduction on Carbonaceous Aerosols? *Geophys. Res. Lett.* **1996**, *23* (19), 2609−2612.

(5) Andreae, M. O.; Rosenfeld, D. Aerosol−Cloud−Precipitation Interactions. Part 1. The Nature and Sources of Cloud-Active Aerosols. *Earth-Sci. Rev.* **2008**, *89* (1−2), 13−41.

(6) (a) Engelstaedter, S.; Tegen, I.; Washington, R. North African Dust Emissions and Transport. *Earth-Sci. Rev.* **2006**, *79* (1−2), 73−100. (b) Moosmüller, H.; Chakrabarty, R. K.; Arnott, W. P. Aerosol Light Absorption and Its Measurement: A Review. *J. Quant. Spectrosc. Radiat. Transfer* **2009**, *110* (11), 844−878.

(7) (a) Dentener, F. J.; Carmichael, G. R.; Zhang, Y.; Lelieveld, J.; Crutzen, P. J. Role of Mineral Aerosol As a Reactive Surface in the Global Troposphere. *J. Geophys. Res.* **1996**, *101* (D17), 22869−22889. (b) Kolb, C. E.; Cox, R. A.; Abbatt, J. P. D.; Ammann, M.; Davis, E. J.; Donaldson, D. J.; Garrett, B. C.; George, C.; Griffiths, P. T.; Hanson, D. R.; Kulmala, M.; McFiggans, G.; Pöschl, U.; Riipinen, I.; Rossi, M. J.; Rudich, Y.; Wagner, P. E.; Winkler, P. M.; Worsnop, D. R.; O'Dowd, C. D. An Overview of Current Issues in the Uptake of Atmospheric Trace Gases by Aerosols and Clouds. *Atmos. Chem. Phys.* **2010**, *10* (21), 10561−10605.

(8) (a) Hand, V. L.; Capes, G.; Vaughan, D. J.; Formenti, P.; Haywood, J. M.; Coe, H. Evidence of Internal Mixing of African Dust and Biomass Burning Particles by Individual Particle Analysis Using Electron Beam Techniques. *J. Geophys. Res.: Atmos.* **2010**, *115*, 10.1029/2009JD012938. (b) Arimoto, R.; Kim, Y. J.; Kim, Y. P.; Quinn, P. K.; Bates, T. S.; Anderson, T. L.; Gong, S.; Uno, I.; Chin, M.; Huebert, B. J.; Clarke, A. D.; Shinozuka, Y.; Weber, R. J.; Anderson, J. R.; Guazzotti, S. A.; Sullivan, R. C.; Sodeman, D. A.; Prather, K. A.; Sokolik, I. N. Characterization of Asian Dust during ACE-Asia. *Global Planet. Change* **2006**, *52* (1−4), 23−56. (c) Kim, K. W.; He, Z. S.; Kim, Y. J. Physicochemical Characteristics and Radiative Properties of Asian Dust Particles Observed at Kwangju, Korea, during the 2001 ACE-Asia Intensive Observation Period. *J. Geophys. Res.: Atmos.* **2004**, *109* (D19), 10.1029/2003JD003693.

(9) (a) Akhter, M. S.; Chughtai, A. R.; Smith, D. M. Reaction of Hexane Soot with Nitrogen Dioxide/Nitrogen Oxide (N_2O_4). *J. Phys. Chem.* **1984**, *88* (22), 5334−5342. (b) Kalberer, M.; Tabor, K.; Ammann, M.; Parrat, Y.; Weingartner, E.; Piguet, D.; Rössler, E.; Jost, D. T.; Türler, A.; Gäggeler, H. W.; Baltensperger, U. Heterogeneous Chemical Processing of $^{13}NO_2$ by Monodisperse Carbon Aerosols at Very Low Concentrations. *J. Phys. Chem.* **1996**, *100* (38), 15487−15493. (c) Rogaski, C. A.; Golden, D. M.; Williams, L. R. Reactive Uptake and Hydration Experiments on Amorphous Carbon Treated with NO_2, SO_2, O_3, HNO_3, and H_2SO_4. *Geophys. Res. Lett.* **1997**, *24* (4), 381−384. (d) Smith, D. M.; Chughtai, A. R. Photochemical Effects in the Heterogeneous Reaction of Soot with Ozone at Low Concentrations. *J. Atmos. Chem.* **1997**, *26* (1), 77−91. (e) Ammann, M.; Kalberer, M.; Jost, D. T.; Tobler, L.; Rossler, E.; Piguet, D.; Gaggeler, H. W.; Baltensperger, U. Heterogeneous Production of Nitrous Acid on Soot in Polluted Air Masses. *Nature* **1998**, *395* (6698), 157−160. (f) Choi, W.; Leu, M.-T. Nitric Acid Uptake and Decomposition on Black Carbon (Soot) Surfaces: Its Implications for the Upper Troposphere and Lower Stratosphere. *J. Phys. Chem. A* **1998**, *102* (39), 7618−7630. (g) Kamm, S.; Möhler, O.; Naumann, K.-H.; Saathoff, H.; Schurath, U. The Heterogeneous Reaction of Ozone with Soot Aerosol. *Atmos. Environ.* **1999**, *33* (28), 4651−4661. (h) Kleffmann, J.; Becker, H.; Lackhoff, K.; Wiesen, M. P. Heterogeneous Conversion of NO_2 on Carbonaceous Surfaces. *Phys. Chem. Chem. Phys.* **1999**, *1* (24), 5443−5450. (i) Longfellow, C. A.; Ravishankara, A. R.; Hanson, D. R. Reactive Uptake on Hydrocarbon Soot: Focus on NO_2. *J. Geophys. Res.* **1999**, *104* (D11), 13833−13840. (j) Al-Abadleh, H. A.; Grassian, V. H. Heterogeneous Reaction of NO_2 on Hexane Soot: A Knudsen Cell and FT-IR Study. *J. Phys. Chem. A* **2000**, *104* (51), 11926−11933. (k) Alcala-Jornod, C.; van den Bergh, H.; Rossi, M. J. Reactivity of NO_2 and H_2O on Soot Generated in the Laboratory: A Diffusion Tube Study at Ambient Temperature. *Phys. Chem. Chem. Phys.* **2000**, *2* (24), 5584−5593. (l) Arens, F.; Ammann, M.; Gutzwiller, L.; Baltensperger, U.; Gäggeler, H. W. Formation of HONO from the Reaction of NO_2 with Diesel Soot. *J. Aerosol Sci.* **2000**, *31* (Suppl. 1), 1035. (m) Stadler, D.; Rossi, M. J. The Reactivity of NO_2 and HONO on Flame Soot at Ambient Temperature: The Influence of Combustion Conditions. *Phys. Chem. Chem. Phys.* **2000**, *2* (23), 5420−5429. (n) Saathoff, H.; Naumann, K.-H; Riemer, N.; Kamm, S.; Mohler, O.; Schurath, U.; Vogel, H.; Vogel, B. The Loss of NO_2, HNO_3, NO_3/N_2O_5, and $HO_2/HOONO_2$ on Soot Aerosol: A Chamber and Modeling Study. *Geophys. Res. Lett.* **2001**, *28* (10), 1957−1960. (o) Prince, A. P.; Wade, J. L.; Grassian, V. H.; Kleiber, P. D.; Young, M. A. Heterogeneous Reactions of Soot Aerosols with Nitrogen Dioxide and Nitric Acid: Atmospheric Chamber and

Knudsen Cell Studies. *Atmos. Environ.* **2002**, *36* (36−37), 5729−5740. (p) Salgado, M. S.; Rossi, M. J. Flame Soot Generated under Controlled Combustion Conditions: Heterogeneous Reaction of NO_2 on Hexane Soot. *Int. J. Chem. Kinet.* **2002**, *34* (11), 620−631. (q) Lelievre, S.; Bedjanian, Y.; Pouvesle, N.; Delfau, J.-L.; Vovelle, C.; Le Bras, G. Heterogeneous Reaction of Ozone with Hydrocarbon Flame Soot. *Phys. Chem. Chem. Phys.* **2004**, *6* (6), 1181−1191. (r) Bedjanian, Y.; Lelievre, S.; Le Bras, G. Experimental Study of the Interaction of HO_2 Radicals with Soot Surface. *Phys. Chem. Chem. Phys.* **2005**, *7* (2), 334−341. (s) Muckenhuber, H.; Grothe, H. The Heterogeneous Reaction between Soot and NO_2 at Elevated Temperature. *Carbon* **2006**, *44* (3), 546−559. (t) Aubin, D. G.; Abbatt, J. P. D. Interaction of NO_2 with Hydrocarbon Soot: Focus on HONO Yield, Surface Modification, and Mechanism. *J. Phys. Chem. A* **2007**, *111* (28), 6263−6273. (u) Hays, M. D.; Vander Wal, R. L. Heterogeneous Soot Nanostructure in Atmospheric and Combustion Source Aerosols. *Energy Fuels* **2007**, *21* (2), 801−811. (v) Karagulian, F.; Rossi, M. J. Heterogeneous Chemistry of the NO_3 Free Radical and N_2O_5 on Decane Flame Soot at Ambient Temperature: Reaction Products and Kinetics. *J. Phys. Chem. A* **2007**, *111* (10), 1914−1926. (w) Khalizov, A. F.; Cruz-Quinones, M.; Zhang, R. Heterogeneous Reaction of NO_2 on Fresh and Coated Soot Surfaces. *J. Phys. Chem. A* **2010**, *114* (28), 7516−7524. (x) Monge, M. E.; D'Anna, B.; Mazri, L.; Giroir-Fendler, A.; Ammann, M.; Donaldson, D. J.; George, C. Light Changes the Atmospheric Reactivity of Soot. *Proc. Natl. Acad. Sci. U.S.A.* **2010**, *107* (15), 6605−6609. (y) Zelenay, V.; Monge, M. E.; D'Anna, B.; George, C.; Styler, S. A.; Huthwelker, T.; Ammann, M. Increased Steady State Uptake of Ozone on Soot due to UV/Vis Radiation. *J. Geophys. Res.: Atmos.* **2011**, *116* (D11), 10.1029/2010JD015500. (z) Han, C.; Liu, Y.; He, H. Heterogeneous Photochemical Aging of Soot by NO_2 under Simulated Sunlight. *Atmos. Environ.* **2012**, *64* (0), 270−276. (aa) Crowley, J. N.; Ammann, M.; Cox, R. A.; Hynes, R. G.; Jenkin, M. E.; Mellouki, A.; Rossi, M. J.; Troe, J.; Wallington, T. J. Evaluated Kinetic and Photochemical Data for Atmospheric Chemistry: Volume V—Heterogeneous Reactions on Solid Substrates. *Atmos. Chem. Phys.* **2010**, *10* (18), 9059−9223. (ab) Lelievre, S.; Bedjanian, Y.; Laverdet, G.; Le Bras, G. Heterogeneous Reaction of NO_2 with Hydrocarbon Flame Soot. *J. Phys. Chem. A* **2004**, *108* (49), 10807−10817.

(10) (a) Guilloteau, A.; Nguyen, M. L.; Bedjanian, Y.; Le Bras, G. Desorption of Polycyclic Aromatic Hydrocarbons from Soot Surface: Pyrene and Fluoranthene. *J. Phys. Chem. A* **2008**, *112* (42), 10552−10559. (b) Bedjanian, Y.; Nguyen, M. L. Kinetics of the Reactions of Soot Surface-Bound Polycyclic Aromatic Hydrocarbons with O_3. *Chemosphere* **2010**, *79* (4), 387−393.

(11) (a) Romanias, M. N.; El Zein, A.; Bedjanian, Y. Heterogeneous Interaction of H_2O_2 with TiO_2 Surface under Dark and UV Light Irradiation Conditions. *J. Phys. Chem. A* **2012**, *116* (31), 8191−8200. (b) Bedjanian, Y.; Romanias, M. N.; El Zein, A. Interaction of OH Radicals with Arizona Test Dust: Uptake and Products. *J. Phys. Chem. A* **2013**, *117* (2), 393−400. (c) Romanias, M. N.; El Zein, A.; Bedjanian, Y. Reactive Uptake of HONO on Aluminium Oxide Surface. *J. Photochem. Photobiol. A* **2012**, *250* (0), 50−57. (d) Romanias, M. N.; El Zein, A.; Bedjanian, Y. Uptake of Hydrogen Peroxide on the Surface of Al_2O_3 and Fe2O_3. *Atmos. Environ.* **2013**, *77* (0), 1−8.

(12) El Zein, A.; Bedjanian, Y. Interaction of NO_2 with TiO_2 Surface under UV Irradiation: Measurements of the Uptake Coefficient. *Atmos. Chem. Phys.* **2012**, *12* (2), 1013−1020.

(13) Bedjanian, Y.; Lelievre, S.; Bras, G. L. Kinetic and Mechanistic Study of the F Atom Reaction with Nitrous Acid. *J. Photochem. Photobiol. A* **2004**, *168* (1−2), 103−108.

(14) (a) Barnard, J. C.; Chapman, E. G.; Fast, J. D.; Schmelzer, J. R.; Slusser, J. R.; Shetter, R. E. An Evaluation of the FAST-J Photolysis Algorithm for Predicting Nitrogen Dioxide Photolysis Rates under Clear and Cloudy Sky Conditions. *Atmos. Environ.* **2004**, *38* (21), 3393−3403. (b) Castro, T.; Ruiz-Squarez, G. L.; Gay, C. Direct Measurement of NO_2 Photolysis Rates for Mexico City. *Atmosfera* **1995**, *8* (4), 137−142. (c) Kraus, A.; Hofzumahaus, A. Field Measurements of Atmospheric Photolysis Frequencies for O_3, NO_2, HCHO, CH_3CHO, H_2O_2, and HONO by UV Spectroradiometry. *J. Atmos. Chem.* **1998**, *31* (1), 161−180.

(15) Bedjanian, Y.; El Zein, A. Interaction of NO_2 with TiO_2 Surface under UV Irradiation: Products Study. *J. Phys. Chem. A* **2012**, *116* (7), 1758−1764.

(16) (a) Guilloteau, A.; Bedjanian, Y.; Nguyen, M. L.; Tomas, A. Desorption of Polycyclic Aromatic Hydrocarbons from a Soot Surface: Three- to Five-Ring PAHs. *J. Phys. Chem. A* **2010**, *114* (2), 942−948. (b) Bedjanian, Y.; Nguyen, M. L.; Guilloteau, A. Desorption of Polycyclic Aromatic Hydrocarbons from Soot Surface: Five- and Six-Ring (C-22, C-24) PAHs. *J. Phys. Chem. A* **2010**, *114* (10), 3533−3539.

(17) Nguyen, M. L.; Bedjanian, Y.; Guilloteau, A. Kinetics of the Reactions of Soot Surface-Bound Polycyclic Aromatic Hydrocarbons with NO_2. *J. Atmos. Chem.* **2009**, *62* (2), 139−150.

(18) (a) Kanakidou, M.; Seinfeld, J. H.; Pandis, S. N.; Barnes, I.; Dentener, F. J.; Facchini, M. C.; Van Dingenen, R.; Ervens, B.; Nenes, A.; Nielsen, C. J.; Swietlicki, E.; Putaud, J. P.; Balkanski, Y.; Fuzzi, S.; Horth, J.; Moortgat, G. K.; Winterhalter, R.; Myhre, C. E. L.; Tsigaridis, K.; Vignati, E.; Stephanou, E. G.; Wilson, J. Organic Aerosol and Global Climate Modelling: A Review. *Atmos. Chem. Phys.* **2005**, *5*, 1053−1123. (b) Brigante, M.; Cazoir, D.; D'Anna, B.; George, C.; Donaldson, D. J. Photoenhanced Uptake of NO_2 by Pyrene Solid Films. *J. Phys. Chem. A* **2008**, *112* (39), 9503−9508.

(19) Stemmler, K.; Ndour, M.; Elshorbany, Y.; Kleffmann, J.; D'Anna, B.; George, C.; Bohn, B.; Ammann, M. Light Induced Conversion of Nitrogen Dioxide into Nitrous Acid on Submicron Humic Acid Aerosol. *Atmos. Chem. Phys.* **2007**, *7* (16), 4237−4248.

(20) (a) Russo, C.; Stanzione, F.; Barbella, R.; Tregrossi, A.; Ciajolo, A. The Characteristics of Soot Formed in Premixed Flames by Different Fuels. *Chem. Eng. Trans.* **2010**, *22*, 41−46. (b) Russo, C.; Stanzione, F.; Alfè, M.; Ciajolo, A.; Tregrossi, A. Spectral Analysis in the UV−Visible Range for Revealing the Molecular Form of Combustion-Generated Carbonaceous Species. *Combust. Sci. Technol.* **2012**, *184* (7−8), 1219−1231.

(21) (a) Standard Reference Data; National Institute of Standards and Technology (NIST): Gaithersburg, MD, 2011. (b) Perkampus, H.-H. *UV−VIS Atlas of Organic Compounds*, 2nd ed.; VCH: Weinheim, Germany, 1992.

(22) Gerecke, A.; Thielmann, A.; Gutzwiller, L.; Rossi, M. J. The Chemical Kinetics of HONO Formation Resulting from Heterogeneous Interaction of NO_2 with Flame Soot. *Geophys. Res. Lett.* **1998**, *25* (13), 2453−2456.

(23) (a) Jain, S. C.; Willander, M.; Kumar, V. *Conducting Organic Materials and Devices*; Semiconductors and Semimetals Series; Elsevier: Amsterdam, 2007; Vol. *81*, pp 1−188. (b) Kim, J. Y.; Lee, K.; Coates, N. E.; Moses, D.; Nguyen, T. Q.; Dante, M.; Heeger, A. J. Efficient Tandem Polymer Solar Cells Fabricated by All-Solution Processing. *Science* **2007**, *317* (5835), 222−225. (c) Rand, B. P.; Xue, J. G.; Uchida, S.; Forrest, S. R. Mixed Donor−Acceptor Molecular Heterojunctions for Photovoltaic Applications. I. Material Properties. *J. Appl. Phys.* **2005**, *98*, 124902-1−124902-7.

(24) (a) Hoex, B.; Gielis, J. J. H.; van de Sanden, M. C. M.; Kessels, W. M. M. On the c-Si Surface Passivation Mechanism by the Negative-Charge-Dielectric Al_2O_3. *J. Appl. Phys.* **2008**, *104* (11), 113703−113707. (b) Singh, V. P.; Singh, R. S.; Parthasarathy, B.; Aguilera, A.; Anthony, J.; Payne, M. Copper-Phthalocyanine-Based Organic Solar Cells with High Open-Circuit Voltage. *Appl. Phys. Lett.* **2005**, *86* (8), 082106-1−082106-3.

(25) Thompson, B. C.; Frechet, J. M. J. Organic Photovoltaics: Polymer−Fullerene Composite Solar Cells. *Angew. Chem., Int. Ed.* **2008**, *47* (1), 58−77.

(26) Singh, V. P.; Parsarathy, B.; Singh, R. S.; Aguilera, A.; Anthony, J.; Payne, M. Characterization of High-Photovoltage CuPc-Based Solar Cell Structures. *Sol. Energy Mater. Sol. Cells* **2006**, *90* (6), 798−812.

(27) Samoilova, R. I.; Dikanov, S. A.; Fionov, A. V.; Tyryshkin, A. M.; Lunina, E. V.; Bowman, M. K. Pulsed EPR Study of Orthophosphoric

and Boric Acid Modified γ-Alumina. *J. Phys. Chem.* **1996**, *100* (44), 17621−17629.
(28) (a) Tabor, K.; Gutzwiller, L.; Rossi, M. J. Heterogeneous Chemical Kinetics of NO_2 on Amorphous Carbon at Ambient Temperature. *J. Phys. Chem.* **1994**, *98* (24), 6172−6186. (b) Tabor, K.; Gutzwiller, L.; Rossi, M. J. The Heterogeneous Interaction of NO_2 with Amorphous Carbon. *Geophys. Res. Lett.* **1993**, *20* (14), 1431−1434.
(29) Frisch, M. J.; Trucks, G. W.; Schlegel, H. B.; Scuseria, G. E.; Robb, M. A.; Cheeseman, J. R.; Scalmani, G.; Barone, V.; Mennucci, B.; Petersson, G. A.; Nakatsuji, H.; Caricato, M.; Li, X.; Hratchian, H. P.; Izmaylov, A. F.; Bloino, J.; Zheng, G.; Sonnenberg, J. L.; Hada, M.; Ehara, M.; Toyota, K.; Fukuda, R.; Hasegawa, J.; Ishida, M.; Nakajima, T.; Honda, Y.; Kitao, O.; Nakai, H.; Vreven, T.; Montgomery, J. A., Jr.; Peralta, J. E.; Ogliaro, F.; Bearpark, M.; Heyd, J. J.; Brothers, E.; Kudin, K. N.; Staroverov, V. N.; Keith, T.; Kobayashi, R.; Normand, J.; Raghavachari, K.; Rendell, A.; Burant, J. C.; Iyengar, S. S.; Tomasi, J.; Cossi, M.; Rega, N.; Millam, J. M.; Klene, M.; Knox, J. E.; Cross, J. B.; Bakken, V.; Adamo, C.; Jaramillo, J.; Gomperts, R.; Stratmann, R. E.; Yazyev, O.; Austin, A. J.; Cammi, R.; Pomelli, C.; Ochterski, J. W.; Martin, R. L.; Morokuma, K.; Zakrzewski, V. G.; Voth, G. A.; Salvador, P.; Dannenberg, J. J.; Dapprich, S.; Daniels, A. D.; Farkas, Ö.; Foresman, J. B.; Ortiz, J. V.; Cioslowski, J.; Fox, D. J. *Gaussian 09*, revision D.01; Gaussian, Inc.: Wallingford, CT, 2009.
(30) Pryor, W. A.; Gleicher, G. J.; Cosgrove, J. P.; Church, D. F. Reaction of Polycyclic Aromatic Hydrocarbons (PAHs) with Nitrogen Dioxide in Solution. Support for an Electron-Transfer Mechanism of Aromatic Nitration Based on Correlations Using Simple Molecular Orbital Theory. *J. Org. Chem.* **1984**, *49* (26), 5189−5194.
(31) (a) Kaupp, G.; Schmeyers, J. Gas/Solid Reactions with Nitrogen Dioxide. *J. Org. Chem.* **1995**, *60* (17), 5494−5503. (b) Shiri, M.; Zolfigol, M. A.; Kruger, H. G.; Tanbakouchian, Z. Advances in the Application of N_2O_4/NO_2 in Organic Reactions. *Tetrahedron* **2010**, *66* (47), 9077−9106.
(32) (a) Woodill, L. A.; Hinrichs, R. Z. Heterogeneous Reactions of Surface-Adsorbed Catechol with Nitrogen Dioxide: Substrate Effects for Tropospheric Aerosol Surrogates. *Phys. Chem. Chem. Phys.* **2010**, *12* (36), 10766−10774. (b) Harrison, M. A. J.; Barra, S.; Borghesi, D.; Vione, D.; Arsene, C.; Olariu, R. L. Nitrated Phenols in the Atmosphere: A Review. *Atmos. Environ.* **2005**, *39* (2), 231−248.
(33) Jia, H.; Zhao, J.; Fan, X.; Dilimulati, K.; Wang, C. Photodegradation of Phenanthrene on Cation-Modified Clays under Visible Light. *Appl. Catal. B: Environ.* **2012**, *123*−*124* (0), 43−51.